

promoting access to White Rose research papers



Universities of Leeds, Sheffield and York
<http://eprints.whiterose.ac.uk/>

This is an author produced version of a paper published in **Biochimica et Biophysica Acta - Biomembranes**.

White Rose Research Online URL for this paper:
<http://eprints.whiterose.ac.uk/11204>

Published paper

Zhang, Z., Pen, Y., Edyvean, R.G., Banwart, S.A., Dalglish, R.M., Geoghegan, M. (2010) *Adhesive and conformational behaviour of mycolic acid monolayers*, Biochimica et Biophysica Acta-Biomembranes, 1798 (9), pp. 1829-1839
<http://dx.doi.org/10.1016/j.bbamem.2010.05.024>

Adhesive and conformational behaviour of mycolic acid monolayers

Zhenyu Zhang,^{†1} Yu Pen,^{1,2} Robert G. Edyvean,² Steven A. Banwart,³ Robert M. Dalglish,⁴ and Mark Geoghegan^{*1}

1. Department of Physics and Astronomy, University of Sheffield, Sheffield S3 7RH, UK
2. Department of Chemical and Process Engineering, University of Sheffield, Sheffield S1 3JD, UK
3. Department of Civil and Structural Engineering, University of Sheffield, Sheffield S1 3JD, UK
4. ISIS Pulsed Neutron and Muon Source, Rutherford Appleton Laboratory, Chilton, Didcot, Oxfordshire OX11 0QX, UK

We have studied the pH-dependent interaction between mycolic acid (MA) monolayers and hydrophobic and hydrophilic surfaces using molecular (colloidal probe) force spectroscopy. In both cases hydrophobic and hydrophilic monolayers (prepared by Langmuir-Blodgett and Langmuir Schaefer deposition on silicon or hydrophobized silicon substrates respectively) were studied. The force spectroscopy data, fitted with classical DLVO (Derjaguin, Landau, Verwey, and Overbeek) theory to examine the contribution of electrostatic and van der Waals forces revealed that electrostatic forces are the dominant contribution to the repulsive force between the approaching colloidal probe and MA monolayers. The good agreement between data and the DLVO model suggest that beyond a few nm away from the surface, hydrophobic, hydration and specific chemical bonding are unlikely to contribute to any significant extent to the interaction energy between the probe and the surface. The pH-dependent conformation of MA molecules in the monolayer at the solid-liquid interface was studied by ellipsometry, neutron reflectometry, and with a quartz crystal microbalance. Monolayers prepared by the Langmuir-Blodgett method demonstrated a distinct pH responsive behaviour, while monolayers prepared by the Langmuir-Schaefer method were less sensitive to pH variation. It was found that the attachment of water molecules plays a vital role in determining the conformation of the MA monolayers.

Keywords: mycolic acid, monolayer, neutron reflectometry, force spectroscopy, DLVO, quartz crystal microbalance

1. Introduction

Members of the genus *Rhodococcus* [1] are well known for their capability to metabolize a variety of pollutants [2, 3], to persist in adverse conditions, and to form biofilms. This makes them suitable microorganisms for the biodegradation of many organic compounds [4]. Bioremediation utilising, for example, various indigenous strains of the genus *Rhodococcus* has proved to be a promising option for the clean-up of polluted sites. Their assimilatory abilities have been attributed to the diversity of their enzymatic activities which are affected by the existence of a mycolic acid monolayer on the cell surface, which may limit the uptake of hydrophobic compounds.

Mycolic acids (MA) are high molecular weight α -alkyl- β -hydroxy fatty acids found in the cell walls of bacteria belonging to the mycolata family of actinomycetes [5, 6], which includes genera such as *Rhodococcus* and *Mycobacterium*. In rhodococci, mycolic acids have between 54 and 60 carbon atoms and may represent up to 40% of the cell wall composition [7, 8]. As a result, rhodococci cells are hydrophobic, allowing adhesion at the oil/water interphase. Furthermore, the cells are able to adapt their membrane composition, in terms of fatty acid composition of the membrane phospholipids, mycolic acid content, and cell wall permeability, in response to the carbon source [9]. The cell envelopes of *Rhodococcus* and *Mycobacterium* have a model structure of a stratified layer that consists of the plasma membrane, peptidoglycan, arabinogalactan, and the outermost membrane [10-12]. The outer membrane was proposed as a lipid bilayer with the inner layer consisting of mycolic acids which are arranged in an orderly fashion, in parallel, and covalently bonded to peptidoglycan via arabinogalactan; and an outer layer of free lipids [10, 13]. Recent studies have shown that the mycobacterial outer membrane is approximately 8 nm thick and is morphologically symmetrical [14, 15]. Although the arrangement and configuration of lipids in the mycobacterial outer membrane are

^{†1} Present address: Department of Chemistry, University of Sheffield, Sheffield S3 7HF, UK

* mark.geoghegan@sheffield.ac.uk

still not fully revealed [16], mycolic acids were found to be indispensable for the structural integrity of the outer membrane [14]. The presence of an MA monolayer has also been correlated with adhesion properties [17]. These properties have attracted much scientific and industrial interest [18-21].

A mycolic acid molecule consists of a long saturated 2-alkyl branch and a long fatty alcohol part known as a 'mero' chain. It has an asymmetric structure about the hydrophilic head group (C-C with COOH and OH) as shown in Fig. 1. Besides their basic structure, mycolic acids extracted from different strains contain diverse functional groups that vary in type, stereochemistry, and spacing. The number of carbon atoms in a mycolic acid molecule also varies between genera [22]. The structures of mycolic acids of genera other than mycobacteria were found to be relatively simple in terms of chemical function, being composed of homologous series. In contrast, mycolic acids of mycobacteria display a large diversity of chain lengths and chemical functions that define the different classes of mycolic acids [23]. Nevertheless, it has been shown that the lipid-rich envelope of mycobacteria could be used as a paradigm for cell envelope organization in the genus *Rhodococcus* because of their similar chemical structures [24, 25].

Atomic force microscopy has been used extensively to study the interaction between microbes and solid surfaces directly by immobilizing bacteria on the substrate or on the AFM cantilever [26]. Another route to further the understanding of the mechanism of bacterial adhesion is to mimic cell and tissue surfaces on solid substrates by deposition of model biomembranes [27-29], ultrathin polymer cushions [30], or extracellular polymers [31, 32]. Measuring the interactions between the MA monolayer and a model surface is critical for understanding microbial adhesion to solid surfaces particularly in relation to biodegradation and bioremediation [33, 34].

Since monolayer molecular aggregation is related to drug permeability via molecular packing, studies have been performed to consider conformation, structure and arrangement of mycolic acid molecules in the Langmuir monolayer on a solid substrate at the air-solid interface [35-41]. Hasegawa et al. [36] investigated the conformation of mycolic acids in a Langmuir-Blodgett monolayer at different surface pressures, and reported that the MA chains take a two or three fold structure; but this study concerned the structure and arrangement of MA molecules in the monolayer, and its topography at the air-solid interface rather than the liquid-solid interface considered in the present work. Although a monolayer of trehalose dimycolate was recently used to manipulate the membranes of mycobacteria [42, 43], few experiments [44, 45] have been performed to explore MA monolayers at the solid-liquid interface, or to simulate microbial adhesion to solid surface by examining the interaction between an MA monolayer and a model surface.

In the present study, mycolic acid monolayers were prepared by two methods; one with the hydrophobic tail exposed at the surface, and the other with the hydrophilic head exposed. These different orientations resulted in different molecular arrangements within the monolayers. Quartz crystal microbalance (QCM), ellipsometry, and neutron scattering methods were utilised to examine the conformation of mixed (keto-, methoxy-, and α -) mycolic acid monolayers at different pH. The results lead to the conclusion that water content is responsible for conformational changes in MA molecules in the monolayer. Interactions between MA monolayers and hydrophobic, or hydrophilic model surfaces have been measured using colloidal probe force spectroscopy. Adhesion forces between the MA monolayer and polystyrene were found to be much greater than that between the MA monolayer and a silica surface. Detailed analyses of the interaction between the MA monolayers and model surfaces were facilitated by a DLVO (after Derjaguin, Landau, Verwey, and Overbeek) analysis.

2. Materials and methods

2.1 Monolayer preparation

Mycolic acid (extracted from *Mycobacterium tuberculosis*, human strain) was used as received from Sigma-Aldrich (M4537-5mg). Silicon (100) wafers (Prolog Semicor Ltd., Ukraine) with native oxide layer intact were used as the substrates for monolayer transfer. The silicon wafers were cut into pieces of approximately 5 cm \times 1 cm and washed in RCA-1 solution (pure water, ammonia and hydrogen peroxide with a volume ratio 5:1:1) at 75°C for 15 minutes to remove any organic contaminants. The

silicon pieces were then rinsed thoroughly with ultrapure water (Elga PURElab option water purifier, 15 M Ω .cm) and dried under nitrogen. Substrates were pre-treated in UV-Ozone (Spectra physics, model 6048, Oriel Instruments, USA) for 15 minutes before Langmuir-Blodgett deposition; or sealed in a Petri dish (overnight) with a limited amount of 1,1,1,3,3,3-hexamethyl-disilazane (HMDS) (Sigma-Aldrich) to form a hydrophobic film as an adhesive layer for Langmuir-Schaefer deposition.

The monolayer transfer was performed using a NIMA LB trough 611D (NIMA Technology Ltd., Coventry, UK), with an initial area 600 cm². 70 μ L mycolic acid/chloroform solution (1 mg mL⁻¹) was spread over an ultrapure water subphase by means of a microsyringe. After the complete evaporation of the chloroform (10-15 minutes), the monolayer film was compressed with a PTFE barrier at a speed of 25 cm² min⁻¹ until the surface pressure of the monolayer reached 25.0 mN m⁻¹.

The monolayer, with its hydrophilic end (3-hydroxy and 2-carboxyl groups) in contact with the underlying silicon substrate and hydrophobic methyl groups on top, was transferred by the Langmuir-Blodgett method (lifting the substrate out of the subphase). The lifting speed of the substrate during LB deposition (vertical dipping) was 0.5 cm min⁻¹. The monolayer with opposite arrangement of molecules (hydrophilic end on top) was transferred by the Langmuir-Schaefer method (lowering the HMDS-functionalised silicon wafer into contact with the compressed monolayer). The monolayer prepared by the LB method will be denoted LB_MA monolayer, while LS_MA indicates a monolayer prepared by the LS method. The transferred monolayers were dried with nitrogen and sealed in nitrogen filled vials.

Film quality was verified by scanning force microscopy (SFM) experiments on the dried MA monolayers (Fig. 2). These surface topography measurements were performed using a Digital Instruments Multimode Nanoscope IIIA (Digital Instruments, Santa Barbara, CA, USA) operating in contact mode with silicon nitride SNL probes (Veeco Probes, Cambridge, U.K.) with a nominal spring constant of 0.12 N m⁻¹ and a nominal tip radius 2 nm.

2.2 Quartz crystal microbalance-dissipation (QCM-D)

The QCM-D measurements were conducted using a Q-Sense D300 system (Q-Sense AB, Gothenburg, Sweden). Silicon coated quartz crystals (5 MHz, AT-cut) were used to transfer LB_MA or LS_MA monolayers. The crystal was mounted in the QCM flow chamber (QAFC301) in which the monolayer was exposed to various pH solutions. Changes in the resonant frequency and the dissipation factor of the crystal were monitored simultaneously at four frequencies (fundamental and three overtones). The shifts from the measurements achieved at 15 MHz (3rd overtone) are presented here due to the increased sensitivity of the signal at this frequency. Loading different pH solutions induces small pressure changes which are observable in the frequency and dissipation traces.

2.3 Ellipsometry

A spectroscopic phase-modulated ellipsometer (UVISEL, HORIBA Jobin Yvon, France) was used to monitor the thickness of LB_MA and LS_MA monolayers in different pH environments. Each monolayer was positioned (on its substrate) in a chamber filled with 40 mL pure water. Sodium hydroxide (NaOH) and hydrogen chloride (HCl) solutions were used to adjust pH which was monitored in situ by a pH meter. The refractive index was taken as 1.48 for the evaluation of monolayer thickness [41]. The thickness of the monolayer was calculated by using WVASE software. A Matlab routine developed in-house was used for parameter fitting of the kinetic measurements, in which changes of monolayer thickness were monitored continuously in various pH environments

2.4 Neutron reflectometry

Neutron reflectivity reveals the scattering length density of a material as a function of distance from a substrate [46]. The scattering length is a nuclear property, and is directly analogous to electron density for x-ray experiments. In our experiments, the scattering length density information can be readily converted into a volume fraction-depth profile if there is significant contrast between the biosurfactant and the water. (The volume fraction-depth profile tells us the fractional volume of the mycolic acid as a function of distance from the substrate.) We use D₂O because its scattering length density is

significantly greater than that of the mycolic acid, whereas that of H₂O is not. LB and LS_MA monolayers were transferred to 50 mm diameter circular silicon wafers and placed in a liquid cell to which the D₂O was added. The pD (here we retain the formal use of pD rather than pH) was altered by the addition of NaOH or HCl to the solution and is considered accurate to within ± 0.5 . The experiments were performed using an inverted geometry, with neutrons incident on the mycolic acid layer through the silicon. The data presented in this paper were obtained using the CRISP reflectometer of the ISIS pulsed neutron source [47] at the Rutherford Appleton Laboratory (Oxfordshire, UK). The scattering length density-depth profile was obtained through the use of an optical matrix analysis [48] using *MOTOFIT* software [49].

2.5 Colloidal probe force spectroscopy

Colloidal probes were prepared by attaching either a silica or polystyrene particle (both with certified mean diameters of 10 μm from Duke Scientific Corporation, California) at the apex of an AFM cantilever (MLCT, Veeco probes) using a minimum of epoxy resin. Each colloidal probe was checked by optical microscopy to verify the position of the particle, both before and after each experiment. Force spectroscopy measurements were performed using a molecular force probe (MFP-1D, Asylum Research Inc., Santa Barbara, USA) on a Halcyonics active vibration table. Control experiments were carried out between colloidal probes and clean silicon wafers to obtain the deflection sensitivity of the cantilever. We used the thermal method to calibrate the spring constant of the cantilever [50]. Each colloidal probe was rinsed in ethanol, dried with nitrogen, and then placed in UV-ozone for at least 20 minutes before each experiment to reduce tip contamination. After laser alignment and loading of the sample surface, 40 μL solution was placed on both the monolayer and cantilever to form a water drop which immersed both substrate and cantilever. In these experiments 1 mM NaCl was used as the supporting electrolyte to screen electrostatic repulsive forces. The experiment was performed after 5-10 minutes giving adequate time for the monolayer to reach equilibrium. The pulling speed of the cantilever was kept constant at 1053 nm s^{-1} for all experiments, with no dwell time on the surface. A loading force of 1 nN was used for the silica probe, and 0.1 nN for the polystyrene probe. Raw data acquired from MFP-1D were converted into force-separation data using a method described previously [51].

3 Results and discussion

3.1 Mycolic acid monolayer deposition

The arrangement of MA molecules in the monolayer at the liquid/air interface is obtained from the surface pressure-molecular area (Π - A) isotherm (Fig. 3). The MA monolayer has a lift-off area (A_{lo}) of 0.85 $\text{nm}^2 \text{molecule}^{-1}$, at which point the molecules begin to interact and exert forces on each other as the space available for the molecules is reduced during compression. The limiting molecular area at which molecules are closely packed and extended by the lateral compression is 0.69 $\text{nm}^2 \text{molecule}^{-1}$, which is obtained by extrapolating the linear part of the isotherm. Cyclic isotherm measurements suggest that molecular rearrangement upon monolayer compression is reversible, although the monolayer collapses at $\Pi > 35 \text{ mN m}^{-1}$. As mycolic acid extracted from *Mycobacterium tuberculosis* was used, it is expected that there are different types of mycolic acids in the monolayer. The lift-off, limiting molecular area and collapse pressure of different types of MAs [37] are compared in Table 1. The lift-off and limiting molecular areas of MA molecules in the present study are 0.85 and 0.69 $\text{nm}^2 \text{molecule}^{-1}$ respectively, which is expected as α - and keto-MAs are the major components in the cell membrane of *M. tb*.

After extensive studies of the conformational behaviour of monolayers of different mycolic acids under compression, Hasegawa and co-workers [37, 38] proposed that α -MA could be expanded to a two-fold structure due to its cyclopropane group being hydrophobic, while keto-MA may take a triple-chain structure, which would not expand under high pressure, as shown in Fig. 4. This hypothesis is supported by a comparison of limiting molecular areas of different MA molecules; the large molecular limiting area of keto-MA suggests that the molecules are not extended at high surface pressure. We

conclude that the monolayers are not uniform in terms of surface topography, chemical composition, and film thickness.

3.2 Quartz crystal microbalance measurements

We show in Fig. 5 changes in frequency (Δf) and dissipation (ΔD) signals when a MA monolayer was exposed to solutions of different pH. The pH was repeatedly switched in the same experiment to check reproducibility. The frequency decreases while dissipation increases when the LB_MA monolayer is exposed to high pH solution, and vice versa (Fig. 5a). Since no further MA was introduced into the system, changes in frequency and dissipation result from either the binding and unbinding of mycolic acid molecules from the supporting substrate, as there is no strong bond between MA and the silicon wafer, or, more likely, due to the presence of water molecules between the monolayer and the substrate or within the monolayer, as has been shown in previous studies [52-56]. The water layer sensed by the crystal can be either 'bound' in the adsorbed molecules, as in the hydration film, or mechanically trapped in cavities on a rough surface; these two contributions being difficult to separate.

If rigid layer behaviour and no slip at the crystal-liquid boundary are assumed, the changes in frequency can be used to measure mass changes on the surface according to the Sauerbrey equation, which is a linear relationship between adsorbed mass, m and Δf [57, 58]. Such an assumption fails to explain mass changes in the high pH environment, which suggests that changes in the viscoelasticity of the hydrodynamic layer (including both the monolayer and the associated hydration layer) in contact with the crystal are also responsible for the observed frequency shifts. The viscosity of the hydrodynamic layer depends on several factors, including interfacial slip associated with the interaction of the monolayer with the solvent and water drag by hydrated molecules at the interface and hydrophobic interactions between the alkyl chains in the monolayer.

The response of the LS_MA monolayer to different pH solutions is shown in Fig. 5b. The changes of both frequency and dissipation are not as distinct as those for the hydrophobic layer. Since the mycolic acid molecules were immobilised on top of the HMDS layer with the hydrophilic end on top, the pH responsive behaviour of the LS_MA monolayer is mainly attributed to the interaction between the carboxylic group and water molecules.

Comparison of the QCM results for both LB_MA and LS_MA monolayers reveals that, although both monolayers display pH-dependent behaviour, the underlying mechanisms are not same; some water molecules are coupled to the carboxylic group in the LS_MA monolayer, whereas a hydration layer is formed between the LB_MA monolayer and the supporting silicon substrate.

It should also be noted that both Δf and ΔD traces did not shift back to the baseline value after being exposed to pH 9.4 solution (Fig. 5a). This can be attributed to trapped water molecules not being released thoroughly. The odd reverse behaviour when the chamber is filled with pH 6.5 solution a second time (at $t = 50$ and 88 min) is hard to understand, but may be due to water molecules being released from the monolayer when the system switches from pH 9.4 to pH 6.5. Although it is expected that there are spikes when loading solutions into the chamber, some changes in both traces are due to temperature fluctuations of the QCM itself, although this is not a large effect. We made every effort to keep the temperature stable, because a fluctuation of 0.04 K could give rise to a fluctuation in Δf of as much as 0.5 Hz.

3.3 Ellipsometry

Ellipsometry experiments were performed with both LB_MA and LS_MA monolayers. The ellipsometric thickness, measured simultaneously when changing solution pH (Fig. 6), is obtained by fitting the experimental data to a model profile, which treats the monolayer as a uniform film. The relative thickness variation with pH confirms the pH-responsive nature of both monolayers, which are both thicker (heavier) at high pH, and compacted at low pH.

3.4 Neutron reflectometry

In principle ellipsometry can provide volume fraction-depth profiles with sub-nm resolution, but in practice neutron reflectometry is a much more powerful tool for obtaining conformational information

about thin layers. The scattering length density of the MA used in this work is a priori unknown because it is a mixture of α , keto, and methoxy mycolic acids. A value of $-2.0 \pm 0.5 \times 10^{-7} \text{ \AA}^{-2}$ was obtained from a consideration of the scattering lengths obtained from these types of MA using a density of 0.9 g/cc, which is typical of similar fatty acids. The large error in the scattering length density of MA is not as important as might be expected, because the D₂O has a much larger scattering length density than that of MA, and so it is the D₂O that is being profiled; the MA essentially being an *absence* of D₂O and the data is verified for consistency by ensuring that the areas under the scattering length density-depth profiles are constant to within $\pm 10\%$.

The model used to fit the data consists of silicon with a scattering length density of $2.07 \times 10^{-6} \text{ \AA}^{-2}$, through which the neutrons passed, incident onto the acid layer. The native oxide layer of the silicon was not removed. This is normally ill defined, but is required to be included in the fitting when one is considering bare substrates, or ultra-thin films, as is the case here. The need for a layer between the mycolic acid and the silicon is especially acute for the hydrophilic MA layer (LS_MA), where the HMDS film complicates the interface between MA and silicon. A difficulty with fitting to an oxide layer is that it is environmentally dependent, because it can be hydrated.

Neutron reflectometry data and fits are shown in Fig. 7 and the corresponding volume fraction-depth profiles for both LB_MA and LS_MA in Fig. 8. There is a difference in profile between the hydrophilic and hydrophobic monolayers, with the hydrophobic LB_MA layers having a more gradual decrease in concentration than the hydrophilic layers at pD 3.0 and 7.0. The LS_MA layer at pD 10 extends into the D₂O much more than any of the other films.

3.5 Colloidal probe measurements: Adhesion force

Adhesion force data for colloidal probes and MA monolayers were collected from individual force curves. Statistical analyses of the adhesion force were based on over 500 force curves, and are shown in Figs 9 and 10. The silica surface has a stronger interaction with both MA monolayers in lower pH solution than at high pH (Fig. 9). For the polystyrene probe, adhesion forces of both hydrophobic and hydrophilic MA were more evenly distributed at pH 6.5 and 10. At pH 3, the adhesion force of LB_MA was mainly weak, with few events exceeding 50 nN, whereas the adhesion force of LS_MA was mainly strong, with a significant number of events exceeding 150 nN at both pH 3 and pH 10 (Fig. 10).

The adhesion force is a combination of electrostatic, van der Waals, and meniscus or capillary forces, as well as chemical bonds or acid-base interactions [59]. For the silica probe, the greater adhesion force in a low pH environment is attributed to the contribution of electrostatic and hydrogen bonding because van der Waals forces are not sensitive to the pH of the solutions. The carbonyl groups (C=O) exposed on the LB_MA monolayer upper surface (from the keto-MA) are weakly positively charged in low pH solution and negatively charged in a high pH environment, whereas the carboxylic acid group (-COOH) exposed on the LS_MA monolayer is negatively charged in high pH solution and less charged in a low pH environment. The silica sphere is negatively charged in a high pH solution and less charged in a low pH solution. It can be concluded that the electrostatic force is repulsive in high pH solution between the silica probe and the monolayers but attractive or less repulsive in low pH solution.

The interaction of MA with the polystyrene probe is stronger than that with the silica probe due to hydrophobic interactions (Fig. 10). There is no strong pH dependence here, except that forces at pH 3.0 are weaker than those at pH 6.0 and 10.0 for the LB_MA. It is perhaps surprising that the hydrophobic effect is even stronger for the LS_MA, when the hydrophilic component is exposed. The interaction is still stronger for the LS_MA at pH 10.0 than pH 6.0. Why the polystyrene probe should have stronger interactions with the LS_MA than with the LB_MA is particularly surprising, but we note that the HMDS underlayer provides more hydrophobic surface than for the LB_MA, where the MA resides on a hydrophilic silica substrate.

3.6 Colloidal probe measurements: Surface potential

The force-distance curves for the approach of silica probe to LB_MA or LS_MA monolayers in 1 mM NaCl solutions of varying pH (3.3, 6.1, and 8.9) are presented in Fig. 11. In Fig. 12, we present equivalent data for the approach of the polystyrene probe to LB_MA or LS_MA in similar solutions at pH 3.0, 6.5, and 10.0. All curves were fitted with standard DLVO theory, which considers only electrostatic double layer and van der Waals forces between the probe and the monolayer, expressed as $F = F_{\text{vdW}} + F_{\text{EDL}}$ [60]. The van der Waals forces were calculated in the form of a sphere interacting with a flat surface, given by

$$F_{\text{vdW}} = \frac{A_{\text{H}}R}{6D^2}, \quad (1)$$

where F_{vdW} is the van der Waals force; R , the radius of the probe; A_{H} , the Hamaker constant; and D , the distance between surfaces. For the silica/water/MA monolayer system, the value of the Hamaker constant (A_{H}) was determined from the distance at the jump-to-contact, D_{jtc} [59],

$$D_{\text{jtc}} = \left(\frac{A_{\text{H}}R}{3k_{\text{c}}} \right)^{1/3}, \quad (2)$$

where k_{c} is the spring constant of the cantilever. The disadvantage of this method is that the Hamaker constant is easily affected by the underlying solid support, although small variations in Hamaker constant do not significantly influence the results. The jump-to-contact distances for the silica probe to LB_MA and LS_MA monolayers were 4.5 and 6.8 nm respectively based on an average of 20 individual force curves; the respective values for the polystyrene probe were 3.5 and 4.8 nm. The calculated Hamaker constants are 3.01×10^{-21} and 1.04×10^{-20} J for LB_MA-silica and LS_MA-silica in water and 1.09×10^{-20} and 2.65×10^{-20} J for LB_MA-polystyrene and LS_MA-polystyrene in water.

The electrostatic interaction energy between the probe and monolayer was calculated by the surface element integration method [61], based on the linearized Poisson-Boltzmann equation under constant potential conditions as derived previously [62]. Finally Derjaguin's approximation ($F/R=2\pi E$) was used to convert the interaction energy, E , to an interaction force, F , between the silica probe and MA monolayer, allowing F_{EDL} to be written as

$$F_{\text{EDL}} = \pi\epsilon\epsilon_0 R\kappa \left(\psi_{\text{s}}^2 + \psi_{\text{p}}^2 \right) \left[1 - \coth(\kappa D) + \frac{2\psi_{\text{s}}\psi_{\text{p}}}{\left(\psi_{\text{s}}^2 + \psi_{\text{p}}^2 \right)} \operatorname{cosech}(\kappa D) \right], \quad (3)$$

where ϵ_0 is the dielectric permittivity of vacuum, ϵ is the dielectric constant of the solvent, ψ_{s} and ψ_{p} are the surface potentials of the probe and monolayer, and κ is the inverse Debye screening length. Eq. (3) can be used to predict the interaction accurately at large separations and also for surfaces with small potentials [63, 64].

During fitting, the Debye length (κ^{-1}) and electric surface potential of the MA monolayer surface (ψ_{s}) were set as adjustable parameters, while the surface potential of silica was set as -21, -40 and -53 mV for pH 3.3, 6.1, and 8.9 respectively, based on previous studies [65-69]. The fitted values of the surface potential of the monolayers and corresponding Debye lengths are summarized in Table 2. Although different polystyrene surface potentials have been proposed [70-73], not all of them have been used to fit force spectroscopy approach curves well. The polystyrene surface potentials presented in Table 3 were obtained by measuring the interaction between a polystyrene probe and a surface coated in polystyrene. The fitted MA surface potentials and Debye lengths are listed in Table 3 for the interaction of MA with polystyrene.

The fitted surface potentials of LB_MA monolayers in pH 6 and pH 9 are very close, which may result from the limited number of carbonyl groups on the surface from the keto-MA (Fig. 4c). It is worth noting that the repulsion between silica/polystyrene probe and LS_MA increases with increasing pH. This can be explained by noting that at high pH the carboxylic groups of MA are negatively charged, whereas at low pH the carboxylic groups are less or even uncharged. Consequently, a clear increase in the surface potential of LS_MA samples with increasing pH is expected. The fitted Debye lengths were

smaller than the calculated value ($\kappa^{-1} = 9.6$ nm) mainly because of the additional ions required to adjust the solution pH [64].

The measured force-distance profiles were fitted reasonably well with standard DLVO theory for both monolayers at separations greater than the Debye length (9.6 nm), suggesting that the long-range repulsive force from the electrostatic double-layer interaction dominates. At distances less than the Debye length, the DLVO analysis deviated from the measured result as it predicted a strong attractive force, which is likely to be due to van der Waals forces dominating against electrostatic repulsive forces. The reason for such failures at small distances is complicated, but could be due to: (i) the nature of the constant potential boundary condition, which deviates from the full solution of non-linear Poisson-Boltzmann curve because of increased attractive forces compared to the constant charge condition that we used at small distances [59, 66]; (ii) additional repulsive forces originating from the hydration of the surfaces [74-76]; (iii) the 'zero distance', which is difficult to define for thicker monolayers, as is the case here in high pH solution; or (iv) surface roughness, which has been demonstrated to affect DLVO interactions [77, 78] but is not taken into account in the present study.

For both LB_MA and LS_MA surfaces against the silica probe, the repulsive force is dominant at high pH, but the attractive force becomes apparent in low pH solution. The long-range repulsive force exists in all environments and has been attributed to an electrostatic double layer repulsive effect. It has been suggested that a hydrous silica gel layer surrounding the silica surface can cause such an interaction at small separations [79]; such short-range attractions have also been attributed to van der Waals forces [80]. In the present study, the reasonable agreement between the DLVO fits and measured results suggests that the attraction is due to van der Waals forces.

The surface potentials will be dependent on pH and the surface in question, and independent of the nature of the probe. The differences between the values of ψ_s presented in Tables 2 and 3 are systematic because they require an accurate Hamaker constant for the interaction between the probe and the surface. This is measured from the jump-to-contact distance of the AFM tip with the surface in the approach curve, and is very sensitive to this distance because the Hamaker constant is proportional to the cube of this distance (Eq. 2) and is also dependent upon the spring constant of the AFM tip. As a result, comparisons between the surface potentials of the different surfaces should be made with caution, but those between the same tip and surface as a function of pH remain valid.

3.7 General discussion

Hasegawa et al. [37] proposed that keto-MA molecules adopt triple-chain folding structures (Fig. 4) due to repulsive intramolecular electrostatic forces between C=O groups, i.e. the mero branch of keto-MA folds at the carbonyl group. The carbonyl group was exposed to aqueous medium in the LB_MA monolayer, and the surface of the hydrophobic MA monolayer is partially covered by this carbonyl group. In the C=O structure, oxygen is more electronegative than carbon, hence oxygen pulls the electron density away from carbon to increase the polarity of the bond. Therefore, the carbonyl carbon becomes electrophilic, and the electronegative oxygen can react with electrophiles such as protons in an acidic solution. On the other hand, the LS_MA monolayer was made to have the carboxylic group on top, which will be negatively charged in high pH solution and less charged (or neutral) at low pH.

It can now be understood why both LB_MA and LS_MA monolayers display similar behaviour in the force measurement experiments. The LB_MA monolayer is neutral in high pH solution, and switches to weakly positively charged in low pH solution, whereas the LS_MA monolayer is negatively charged at high pH and neutral in the low pH environment. The values of surface potential obtained from DLVO fitting reflect all of these chemical changes.

In analyzing the whole force curve for the interactions with silica, there is hysteresis between the approach and retraction parts when there are strong attractive forces between the probe and sample surface, and no hysteresis when both surfaces repel each other. The likelihood of such hysteresis is much greater for both MA monolayers against the silica probe in pH 3.3 solution than for higher pH, which confirms that the surfaces are less negatively charged. The adhesion force between the silica probe and the hydrophilic MA monolayer is greater than the hydrophobic monolayer in the low pH

solution, which can be attributed to the formation of hydrogen bonds between the carboxylic group and the silanol group on the silica sphere. This hysteresis was not observed with the polystyrene probe, which cannot form hydrogen bonds with the hydrophilic MA monolayer.

The increased thickness of the LS_MA monolayer in high pH solution is attributed to the dissociation of carboxylic acid groups which generates more space between MA molecules to enable the accommodation of water molecules. Both carboxylic and silanol groups are negatively charged at high pH, and therefore there is a repulsive force between the bottom of the LB_MA monolayer and the underlying silicon surface, which offers the opportunity for water molecules to form a hydration layer here (Fig. 13). The distinct mass changes of LB_MA in high pH conditions are due to the formation of such a hydration layer.

Under compression by the colloidal probe, the water trapped within and under the MA monolayer is squeezed out of the layer. The osmotic repulsive force caused by the compression of the hydrodynamic layer (which includes both the MA monolayer and the hydration layer) depends on the water content within the layer. The water content can be estimated from force curves based on a consideration of the compression of the hydrodynamic layer from a fully hydrated state to a “dry” state. Here, the decrease in thickness reveals the degree of hydration. Such a compression phenomenon happens with LB_MA and LS_MA monolayers only in pH 8.9 solution, supporting the QCM, ellipsometry, and neutron reflectometry results, which all show that the monolayers are hydrated in a high pH environment.

The possibility of the precipitation of sodium ions on the silicon substrate cannot be ignored because 1 mM sodium chloride solution was used as background in all measurements. The hydroxyl groups on a hydrous oxide have donor properties, and therefore the sorption of sodium ions and protons can be understood as a competitive complex formation with de-protonated surface groups (Si-O⁻) in high pH environments. However, no obvious changes have been observed from the control experiments of the bare silicon substrate, which means the possibility of precipitation can be excluded in the present study.

4 Conclusions

Colloidal probe force measurements on mycolic acid monolayers (hydrophobic and hydrophilic) on silicon wafers (HMDS-coated for hydrophilic films) have provided information on both the total surface forces and the components contributing to the net force. The measured interfacial forces can be interpreted in terms of contributions that depend on the surface chemistry of the monolayer as well as the pH of the solutions that measurements were taken in. From fitting to classical DLVO theory it can be concluded that: (i) van der Waals forces play a minor role and do not contribute significantly to the interaction with the surface; (ii) the electrostatic double-layer force is the main contribution to the long-range repulsive interaction; and (iii) the deviation of the DLVO theoretical curve from the experimental data at small distances ($< \kappa^{-1}$) is due to repulsion upon compression of the hydrated monolayer, which is not included in the classical DLVO theory. The adhesion between the MA monolayers and the polystyrene surface were found to be much stronger than that between the MA monolayers and a silica surface. These results can be applied to explain phenomena of the outer layer of the cell membrane. The differences between LB_MA and LS_MA and the pH sensitivity demonstrate the scope for explaining different cell adhesion properties in different mycobacteria.

The results support the validity of the “triple-folded” structure of keto-MA in Langmuir-Blodgett monolayers, and that the exposure of the carbonyl group to an aqueous medium leads to the appearance of a significant electrostatic contribution to the net surface force. Although both LB_MA and LS_MA monolayers were hydrated in high pH solution, they have different hydration mechanisms: at high pH, a hydration layer is formed between a LB_MA monolayer and the underlying silicon substrate or on top of the LS_MA monolayer, whereas both LB and LS_MA monolayers are compact and rigid at low pH due to the loss of the hydration layer.

Acknowledgements. We thank Dr Tim Richardson for the use of the Langmuir trough and Mr Mike Weir for help with the fitting of the ellipsometry data. Funding from the EPSRC GR/S74267/01 is gratefully acknowledged.

Tables

	Lift-off molecular area (nm ²)	Limiting molecular area (nm ²)	Collapse surface pressure (mN m ⁻¹)
α -MA (<i>M. tb</i>)	0.63	0.48	20
Keto-MA (<i>M. tb</i>)	0.90	0.77	40
Methoxy-MA (<i>M. tb</i>)	0.80	0.64	20

Table 1. Comparison of the surface pressure-molecular area (Π - A) isotherm results of different MAs extracted from *M. tb* [37].

	Surface potential, ζ (mV)			Debye length, λ^{-1} (nm)
	pH 3.3	pH 6.1	pH 8.9	
Silica probe	-21	-40	-53	
LB_MA	-8.6 \pm 0.1	-17.6 \pm 0.1	-18.4 \pm 0.4	6.7
LS_MA	-8.6 \pm 0.1	-18.9 \pm 0.2	-25.3 \pm 0.2	5.1

Table 2. Surface potential values of LB_MA and LS_MA monolayers in different pH environments calculated by DLVO fitting for experiments in which a silica probe was used.

	Surface potential, ζ (mV)			Debye length, λ^{-1} (nm)
	pH 3.0	pH 6.5	pH 10.0	
Polystyrene probe	-13.2	-26.1	-28.8	
LB_MA	-5.2 \pm 0.1	-21.9 \pm 0.6	-18.7 \pm 0.2	7.0
LS_MA	-21.6 \pm 0.6	-33.6 \pm 0.3	-38.6 \pm 0.3	8.0

Table 3. MA surface potentials and Debye lengths for the interaction of mycolic acid monolayers with a polystyrene probe.

Figure captions

Fig. 1. Generic molecular structure of mycolic acids, in which k , l , m , and n represent the number of carbon atoms; $k = 21$ or 23 , and l , m , and n vary depending on the MA. R_1 corresponds to *cis*-cyclopropyl for ζ -MA, $\text{CH}(\text{CH}_3)\text{-CO}$ for keto-MA, and $\text{CH}(\text{CH}_3)\text{-CH}(\text{OCH}_3)$ for methoxy-MA. R_2 is a cyclopropyl group, which is *cis* for ζ -MA and may be either *cis* or *trans* for keto- or methoxy-MA.

Fig. 2. SFM height images of MA monolayers on a silicon wafer prepared by (a) Langmuir-Blodgett, and (b) Langmuir-Schafer methods at a surface pressure of 25.0 mN m^{-1} . (c) Height scans for the lines marked in (a) and (b). (The two lines are scaled with respect to each other for clarity; the absolute values of height are unimportant.)

Fig. 3. Surface pressure-area (Π - A) isotherm of mixed mycolic acids of average molecular mass 1.3 kg mol^{-1} on pure water at 25°C . The broken line denotes the limiting area per molecule at which the molecules are close packed ($0.69 \text{ nm}^2 \text{ molecule}^{-1}$).

Fig. 4. Schematic diagram of the unfolding mechanism of MA by lateral pressure. (a) Triple-chain structure of ζ -MA molecule at low pressure in which the short-branch partially interacts with the mero group. (b) Double-chain structure of ζ -MA molecule at high pressure, the mero group is extended, and the short branch does not readily interact with the linear part of the mero branch. (c) Triple-chain structure of keto-MA molecule at all surface pressures [37].

Fig. 5. QCM-D measurements of the frequency, $\otimes f$, (grey circles) and dissipation, $\otimes D$ (solid line) shifts corresponding to changes in pH for (a) hydrophobic and (b) hydrophilic monolayers.

Fig. 6. Thickness of (a) hydrophobic and (b) hydrophilic MA monolayers for different pH, monitored by in situ ellipsometry.

Fig. 7. Neutron reflectivity, R data and fits as a function of Q (twice the perpendicular component of the neutron wave vector or the momentum transfer divided by \hbar) for (a) LB and (b) LS_MA monolayers. The inset shows the scattering length density (SLD)-depth profile. A scattering length density of $6.36 \times 10^{-2} \text{ \AA}^{-2}$ is that of pure D_2O and one of $2.07 \times 10^{-2} \text{ \AA}^{-2}$ is silicon.

Fig. 8. Volume fraction-depth profiles for the (a) LB and (b) LS_MA monolayers. These profiles are strongly related to the scattering length density profiles shown in the insets to Fig. 7.

Fig. 9. Statistical analysis of adhesion forces between a silica colloidal probe and (a) a LB_MA monolayer and (b) a LS_MA monolayer for three different pH environments.

Fig. 10. Statistical analysis of adhesion forces between a polystyrene colloidal probe and (a) a LB_MA monolayer and (b) a LS_MA monolayer for three different pH environments.

Fig. 11. Force-distance curves for the approach of a silica probe to (a) LB_MA monolayer and (b) LS_MA monolayer in different pH environments. The data are fitted (broken lines) to the DLVO equation.

Fig. 12. Force-distance curves for the approach of a polystyrene probe to (a) LB_MA monolayer and (b) LS_MA monolayer in different pH environments. The data are fitted (broken lines) to the DLVO equation.

Fig. 13. Schematic illustration of hydration mechanism of: LB_MA monolayer in (a) pH ~ 3 , (b) pH ~ 6 , (c) pH ~ 9 solutions; and LS_MA monolayer in (d) pH ~ 3 , (e) pH ~ 6 , (f) pH ~ 9 solutions.

References

- [1] V. Gürtler, B.C. Mayall, R. Seviour, Can whole genome analysis refine the taxonomy of the genus *Rhodococcus*?, FEMS Microbiol. Rev. 28 (2004) 377-403.
- [2] A. Banerjee, R. Sharma, U.C. Banerjee, The nitrile-degrading enzymes: current status and future prospects, Appl. Microbiol. Biotechnol. 60 (2002) 33-44.
- [3] L. Martínková, B. Uhnáková, M. Pátek, J. Nešvera, V. Křen, Biodegradation potential of the genus *Rhodococcus*, Environ. Int. 35 (2009) 162-177.
- [4] L.G. Whyte, J. Hawari, E. Zhou, L. Bourbonnière, W.E. Inniss, C.W. Greer, Biodegradation of variable-chain-length alkanes at low temperatures by a psychrotrophic *Rhodococcus* sp., Appl. Environ. Microbiol. 64 (1998) 2578-2584.
- [5] T.R. Paul, T.J. Beveridge, Reevaluation of envelope profiles and cytoplasmic ultrastructure of mycobacteria processed by conventional embedding and freeze-substitution protocols, J. Bacteriol. 174 (1992) 6508-6517.
- [6] M.R. McNeil, P.J. Brennan, Structure, function and biogenesis of the cell envelope of mycobacteria in relation to bacterial physiology, pathogenesis and drug resistance; some thoughts and possibilities arising from recent structural information, Res. Microbiol. 142 (1991) 451-463.
- [7] C.E. Barry III, R.E. Lee, K. Mdluli, A.E. Sampson, B.G. Schroeder, R.A. Slayden, Y. Yuan, Mycolic acids: structure, biosynthesis and physiological functions, Prog. Lipid Res. 37 (1998) 143-179.
- [8] M. Watanabe, Y. Aoyagi, H. Mitome, T. Fujita, H. Naoki, M. Ridell, D.E. Minnikin, Location of functional groups in mycobacterial meromycolate chains; the recognition of new structural principles in mycolic acids, Microbiology 148 (2002) 1881-1902.
- [9] I. Sokolovská, R. Rozenberg, C. Riez, P.G. Rouxhet, S.N. Agathos, P. Wattiau, Carbon source-induced modifications in the mycolic acid content and cell wall permeability of *Rhodococcus erythropolis* E1, Appl. Environ. Microbiol. 69 (2003) 7019-7027.
- [10] D.E. Minnikin, Chemical principles in the organization of lipid components in the mycobacterial cell envelope, Res. Microbiol. 142 (1991) 423-427.
- [11] M. McNeil, M. Daffe, P.J. Brennan, Location of the mycolyl ester substituents in the cell walls of mycobacteria, J. Biol. Chem. 266 (1991) 13217-13223.
- [12] T.R. Paul, T.J. Beveridge, Preservation of surface lipids and determination of ultrastructure of *Mycobacterium kansasii* by freeze-substitution, Infect. Immun. 62 (1994) 1542-1550.
- [13] B.A. Dmitriev, S. Ehlers, E.T. Rietschel, P.J. Brennan, Molecular mechanics of the mycobacterial cell wall: From horizontal layers to vertical scaffolds, Int. J. Med. Microbiol. 290 (2000) 251-258.

- [14] C. Hoffmann, A. Leis, M. Niederweis, J.M. Plitzko, H. Engelhardt, Disclosure of the mycobacterial outer membrane: Cryo electron tomography and vitreous sections reveal the lipid bilayer structure, *Proc. Natl Acad. Sci. USA* 105 (2008) 3963-3967.
- [15] B. Zuber, M. Chami, C. Houssin, J. Dubochet, G. Griffiths, M. Daffé, Direct visualization of the outer membrane of mycobacteria and corynebacteria in their native state, *J. Bacteriol.* 190 (2008) 5672-5680.
- [16] M. Niederweis, O. Danilchanka, J. Huff, C. Hoffmann, H. Engelhardt, Mycobacterial outer membranes: in search of proteins, *Trends Microbiol.* 18 (2010) 109-116.
- [17] B. Bendinger, H.H.M. Rijnaarts, K. Altendorf, A.J.B. Zehnder, Physicochemical cell surface and adhesive properties of coryneform bacteria related to the presence and chain length of mycolic acids, *Appl. Environ. Microbiol.* 59 (1993) 3973-3977.
- [18] M. Faller, M. Niederweis, G.E. Schulz, The structure of a mycobacterial outer-membrane channel, *Science* 303 (2004) 1189-1192.
- [19] X. Hong, A.J. Hopfinger, Construction, molecular modeling, and simulation of mycobacterium tuberculosis cell walls, *Biomacromolecules* 5 (2004) 1052-1065.
- [20] H.M. Stratton, P.R. Brooks, P.C. Griffiths, R.J. Seviour, Cell surface hydrophobicity and mycolic acid composition of *Rhodococcus* strains isolated from activated sludge foam, *J. Ind. Microbiol. Biotech.* 28 (2002) 264-267.
- [21] M.P. McLeod, R.L. Warren, W.W.L. Hsiao, N. Araki, M. Myhre, C. Fernandes, D. Miyazawa, W. Wong, A.L. Lillquist, D. Wang, M. Dosanjh, H. Hara, A. Petrescu, R.D. Morin, G. Yang, J.M. Stott, J.E. Schein, H. Shin, D. Smailus, A.S. Siddiqui, M.A. Marra, S.J.M. Jones, R. Holt, F.S.L. Brinkman, K. Miyauchi, M. Fukuda, J.E. Davies, W.W. Mohn, L.D. Eltis, The complete genome of *Rhodococcus* sp. RHA1 provides insights into a catabolic powerhouse, *Proc. Natl Acad. Sci. USA* 103 (2006) 15582-15587.
- [22] M. Goodfellow, L.A. Maldonado, The families Dietziaceae, Gordoniaceae, Nocardiaceae and Tsukamurellaceae, in: M. Dworkin, S. Falkow, E. Rosenberg, K.-H. Schleifer, E. Stackebrandt (Eds.), *The Prokaryotes*, vol. 3, Springer, New York, 2006, pp. 843-888.
- [23] H. Marrakchi, F. Bardou, M.-A. Lanéelle, M. Daffé, A comprehensive overview of mycolic acid structure and biosynthesis, in: M. Daffé, J.-M. Reyrat (Eds.), *The Mycobacterial Cell Envelope*, ASM Press, Washington DC, 2008.
- [24] D.E. Minnikin, A.G. O'Donnell, Actinomycete envelope lipids and peptidoglycan composition, in: M. Goodfellow, M. Mordarski, S.T. Williams (Eds.), *The Biology of the Actinomycetes*, Academic Press, London, 1984, pp. 337-388.
- [25] I.C. Sutcliffe, Macroamphiphilic cell envelope components of *Rhodococcus equi* and closely related bacteria, *Vet. Microbiol.* 56 (1997) 287-299.
- [26] T.A. Camesano, Y. Liu, M. Datta, Measuring bacterial adhesion at environmental interfaces with single-cell and single-molecule techniques, *Adv. Water Resour.* 30 (2007) 1470-1491.
- [27] Y.F. Dufrêne, T. Boland, J.W. Schneider, W.R. Barger, G.U. Lee, Characterization of the physical properties of model biomembranes at the nanometer scale with the atomic force microscope, *Faraday Discuss.* 111 (1998) 79-94.
- [28] Y.F. Dufrêne, G.U. Lee, Advances in the characterization of supported lipid films with the atomic force microscope, *Biochim. Biophys. Acta* 1509 (2000) 14-41.
- [29] L. Picas, C. Suárez-Germà, M.T. Montero, J. Hernández-Borrell, Force spectroscopy study of Langmuir-Blodgett asymmetric bilayers of phosphatidylethanolamine and phosphatidylglycerol, *J. Phys. Chem. B* 114 (2010) 3543-3549.
- [30] K. Sengupta, J. Schilling, S. Marx, M. Fischer, A. Bacher, E. Sackmann, Mimicking tissue surfaces by supported membrane coupled ultrathin layer of hyaluronic acid, *Langmuir* 19 (2003) 1775-1781.
- [31] G.A. Burks, S.B. Velegol, E. Paramonova, B.E. Lindenmuth, J.D. Feick, B.E. Logan, Macroscopic and nanoscale measurements of the adhesion of bacteria with varying outer layer surface composition, *Langmuir* 19 (2003) 2366-2371.
- [32] L.-C. Xu, B.E. Logan, Interaction forces measured using AFM between colloids and surfaces coated with both dextran and protein, *Langmuir* 22 (2006) 4720-4727.
- [33] J.S. Andrews, S. Rolfe, W. Huang, J. Scholes, S.A. Banwart, Biofilm formation in environmental bacteria is influenced by different macromolecules depending on genus and species, *Environ. Microbiol.* 12 (2010) 10.1111/j.1462-2920.2010.02223.x.
- [34] M. Geoghegan, J.S. Andrews, C.A. Biggs, K.E. Eboigbodin, D.R. Elliott, S. Rolfe, J. Scholes, J.J. Ojeda, M.E. Romero-González, R.G.J. Edyvean, L. Swanson, R. Rutkaite, R. Fernando, Y. Pen, Z. Zhang, S.A. Banwart, The polymer physics and chemistry of microbial cell attachment and adhesion, *Faraday Discuss.* 139 (2008) 85-103.
- [35] G. Chimote, R. Banerjee, Inhibitory effects of mycobacterial cell wall lipids on bovine lung surfactant extract: An *in vitro* study at the air-aqueous interface, *Colloids Surf. A* 338 (2009) 7-14.

- [36] T. Hasegawa, S. Amino, S. Kitamura, L. Matsumoto, S. Katada, J. Nishijo, Study of the molecular conformation of α - and keto-mycolic acid monolayers by the Langmuir-Blodgett technique and Fourier transform infrared reflection-absorption spectroscopy, *Langmuir* 19 (2003) 105-109.
- [37] T. Hasegawa, R.M. Leblanc, Aggregation properties of mycolic acid molecules in monolayer films: a comparative study of compounds from various acid-fast bacterial species, *Biochim. Biophys. Acta* 1617 (2003) 89-95.
- [38] T. Hasegawa, J. Nishijo, M. Watanabe, K. Funayama, T. Imae, Conformational characterization of α -mycolic acid in a monolayer film by the Langmuir-Blodgett technique and atomic force microscopy, *Langmuir* 16 (2000) 7325-7330.
- [39] T. Hasegawa, J. Nishijo, M. Watanabe, J. Umemura, Y. Ma, G. Sui, Q. Huo, R.M. Leblanc, Characteristics of long-chain fatty acid monolayers studied by infrared external-reflection spectroscopy, *Langmuir* 18 (2002) 4758-4764.
- [40] M. Villeneuve, M. Kawai, H. Kanashima, M. Watanabe, D.E. Minnikin, H. Nakahara, Temperature dependence of the langmuir monolayer packing of mycolic acids from *Mycobacterium tuberculosis*, *Biochim. Biophys. Acta* 1715 (2005) 71-80.
- [41] M. Villeneuve, M. Kawai, M. Watanabe, Y. Aoyagi, Y. Hitotsuyanagi, K. Takeya, H. Gouda, S. Hirono, D.E. Minnikin, H. Nakahara, Conformational behavior of oxygenated mycobacterial mycolic acids from *Mycobacterium bovis* BCG, *Biochim. Biophys. Acta* 1768 (2007) 1717-1726.
- [42] C.W. Harland, D. Rabuka, C.R. Bertozzi, R. Parthasarathy, The *Mycobacterium tuberculosis* virulence factor trehalose dimycolate imparts desiccation resistance to model mycobacterial membranes, *Biophys. J.* 94 (2008) 4718-4724.
- [43] C.W. Harland, Z. Botyanszki, D. Rabuka, C.R. Bertozzi, R. Parthasarathy, Synthetic trehalose glycolipids confer desiccation resistance to supported lipid monolayers, *Langmuir* 25 (2009) 5193-5198.
- [44] N.S. Mathebula, J. Pillay, G. Toschi, J.A. Verschoor, K.I. Ozoemena, Recognition of anti-mycolic acid antibody at self-assembled mycolic acid antigens on a gold electrode: a potential impedimetric immunosensing platform for active tuberculosis, *Chem. Commun.* (2009) 3345-3347.
- [45] K.I. Ozoemena, N.S. Mathebula, J. Pillay, G. Toschi, J.A. Verschoor, Electron transfer dynamics across self-assembled N-(2-mercaptoethyl) octadecanamide/mycolic acid layers: impedimetric insights into the structural integrity and interaction with anti-mycolic acid antibodies, *Phys. Chem. Chem. Phys.* 12 (2010) 345-357.
- [46] J. Penfold, R.K. Thomas, The application of the specular reflection of neutrons to the study of surfaces and interfaces, *J. Phys.: Condens. Matter* 2 (1990) 1369-1412.
- [47] J. Penfold, R.C. Ward, W.G. Williams, A Time-of-Flight neutron reflectometer for surface and interfacial studies, *J. Phys. E: Sci. Instrum.* 20 (1987) 1411-1417.
- [48] O.S. Heavens, *Optical properties of thin solid films*, Butterworths, London, 1955.
- [49] A. Nelson, Co-refinement of multiple-contrast neutron/X-ray reflectivity data using *MOTOFIT*, *J. Appl. Crystallogr.* 39 (2006) 273-276.
- [50] J.L. Hutter, J. Bechhoefer, Calibration of atomic-force microscope tips, *Rev. Sci. Instrum.* 64 (1993) 1868-1873.
- [51] J. Seog, D. Dean, A.H.K. Plaas, S. Wong-Palms, A.J. Grodzinsky, C. Ortiz, Direct measurement of glycosaminoglycan intermolecular interactions via high-resolution force spectroscopy, *Macromolecules* 35 (2002) 5601-5615.
- [52] K. Ariga, Y. Okahata, Hydration behavior of phospholipid Langmuir-Blodgett (LB) films deposited on a quartz-crystal microbalance depending on temperatures in water, *Langmuir* 10 (1994) 2272-2276.
- [53] Y.-L. Chen, J.N. Israelachvili, Effects of ambient conditions on adsorbed surfactant and polymer monolayers, *J. Phys. Chem.* 96 (1992) 7752-7760.
- [54] M.T. Colberg, A.E. Sáez, C.S. Grant, K. Hutchison, D. Hesterberg, Dynamic hydration of phospholipid films in aqueous environments, *Colloids Surf. A* 151 (1999) 483-495.
- [55] M.L. Gee, J.N. Israelachvili, Interactions of surfactant monolayers across hydrocarbon liquids, *J. Chem. Soc. Faraday Trans. 86* (1990) 4049-4058.
- [56] T.J. Zwang, W.R. Fletcher, T.J. Lane, M.S. Johal, Quantification of the layer of hydration of a supported lipid bilayer, *Langmuir* 26 (2010) 4598-4601.
- [57] M. Rodahl, F. Höök, B. Kasemo, QCM operation in liquids: An explanation of measured variations in frequency and Q factor with liquid conductivity, *Anal. Chem.* 68 (1996) 2219-2227.
- [58] G. Sauerbrey, The use of quartz oscillators for weighing thin layers and for microweighing, *Z. Phys.* 155 (1959) 206-222.
- [59] H.-J. Butt, B. Cappella, M. Kappl, Force measurements with the atomic force microscope: Technique, interpretation and applications, *Surf. Sci. Rep.* 59 (2005) 1-152.
- [60] J.N. Israelachvili, *Intermolecular and surface forces*, 2nd ed., Academic Press, London, 1992.
- [61] S. Bhattacharjee, M. Elimelech, Surface element integration: A novel technique for evaluation of DLVO interaction between a particle and a flat plate, *J. Colloid Interface Sci.* 193 (1997) 273-285.

- [62] R. Hogg, T.W. Healy, D.W. Fuerstenau, Mutual coagulation of colloidal dispersions, *Trans. Faraday Soc.* 62 (1966) 1638-1651.
- [63] P.K. Das, S. Bhattacharjee, Electrostatic double layer force between a sphere and a planar substrate in the presence of previously deposited spherical particles, *Langmuir* 21 (2005) 4755-4764.
- [64] H. Zhao, S. Bhattacharjee, R. Chow, D. Wallace, J.H. Masliyah, Z. Xu, Probing surface charge potentials of clay basal planes and edges by direct force measurements, *Langmuir* 24 (2008) 12899-12910.
- [65] P.G. Hartley, I. Larson, P.J. Scales, Electrokinetic and direct force measurements between silica and mica surfaces in dilute electrolyte solutions, *Langmuir* 13 (1997) 2207-2214.
- [66] I. Larson, C.J. Drummond, D.Y.C. Chan, F. Grieser, Direct force measurements between dissimilar metal oxides, *J. Phys. Chem.* 99 (1995) 2114-2118.
- [67] J. Long, L. Zhang, Z. Xu, J.H. Masliyah, Colloidal interactions between Langmuir-Blodgett bitumen films and fine solid particles, *Langmuir* 22 (2006) 8831-8839.
- [68] G. Toikka, R.A. Hayes, Direct measurement of colloidal forces between mica and silica in aqueous electrolyte, *J. Colloid Interface Sci.* 191 (1997) 102-109.
- [69] N.C. Woodward, M.J. Snowden, B.Z. Chowdhry, P. Jenkins, I. Larson, Measurement of the interaction forces between Poly(*N*-isopropylacrylamide-acrylic acid) microgel and silica surfaces by colloid probe microscopy, *Langmuir* 18 (2002) 2089-2095.
- [70] Y.Q. Li, N.J. Tao, J. Pan, A.A. Garcia, S.M. Lindsay, Direct measurement of interaction forces between colloidal particles using the scanning force microscope, *Langmuir* 9 (1993) 637-641.
- [71] O.I. Vinogradova, G.E. Yakubov, H.-J. Butt, Forces between polystyrene surfaces in water-electrolyte solutions: Long-range attraction of two types?, *J. Chem. Phys.* 114 (2001) 8124-8131.
- [72] L.-C. Xu, B.E. Logan, Interaction forces between colloids and protein-coated surfaces measured using an atomic force microscope, *Environ. Sci. Technol.* 39 (2005) 3592-3600.
- [73] E.C.Y. Yan, Y. Liu, K.B. Eisenthal, New method for determination of surface potential of microscopic particles by second harmonic generation, *J. Phys. Chem. B* 102 (1998) 6331-6336.
- [74] M. Boström, D.R.M. William, B.W. Ninham, Specific ion effects: Why DLVO theory fails for biology and colloid systems, *Phys. Rev. Lett.* 87 (2001) 168103
- [75] A. Grabbe, R.G. Horn, Double-layer and hydration forces measured between silica sheets subjected to various surface treatments, *J. Colloid Interface Sci.* 157 (1993) 375-383.
- [76] G. Vigil, Z. Xu, S. Steinberg, J. Israelachvili, Interactions of silica surfaces, *J. Colloid Interface Sci.* 165 (1994) 367-385.
- [77] S. Bhattacharjee, C.-H. Ko, M. Elimelech, DLVO interaction between rough surfaces, *Langmuir* 14 (1998) 3365-3375.
- [78] E.M.V. Hoek, G.K. Agarwal, Extended DLVO interactions between spherical particles and rough surfaces, *J. Colloid Interface Sci.* 298 (2006) 50-58.
- [79] K.E. Bremmell, G.J. Jameson, S. Biggs, Polyelectrolyte adsorption at the solid/liquid interface Interaction forces and stability, *Colloids Surf. A* 139 (1998) 199-211.
- [80] O. Teschke, G. Ceotto, E.F. de Souza, Interfacial water dielectric-permittivity-profile measurements using atomic force microscopy, *Phys. Rev. E* 64 (2001) 011605

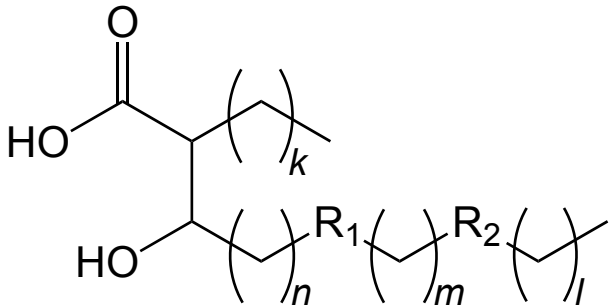


Figure 2a

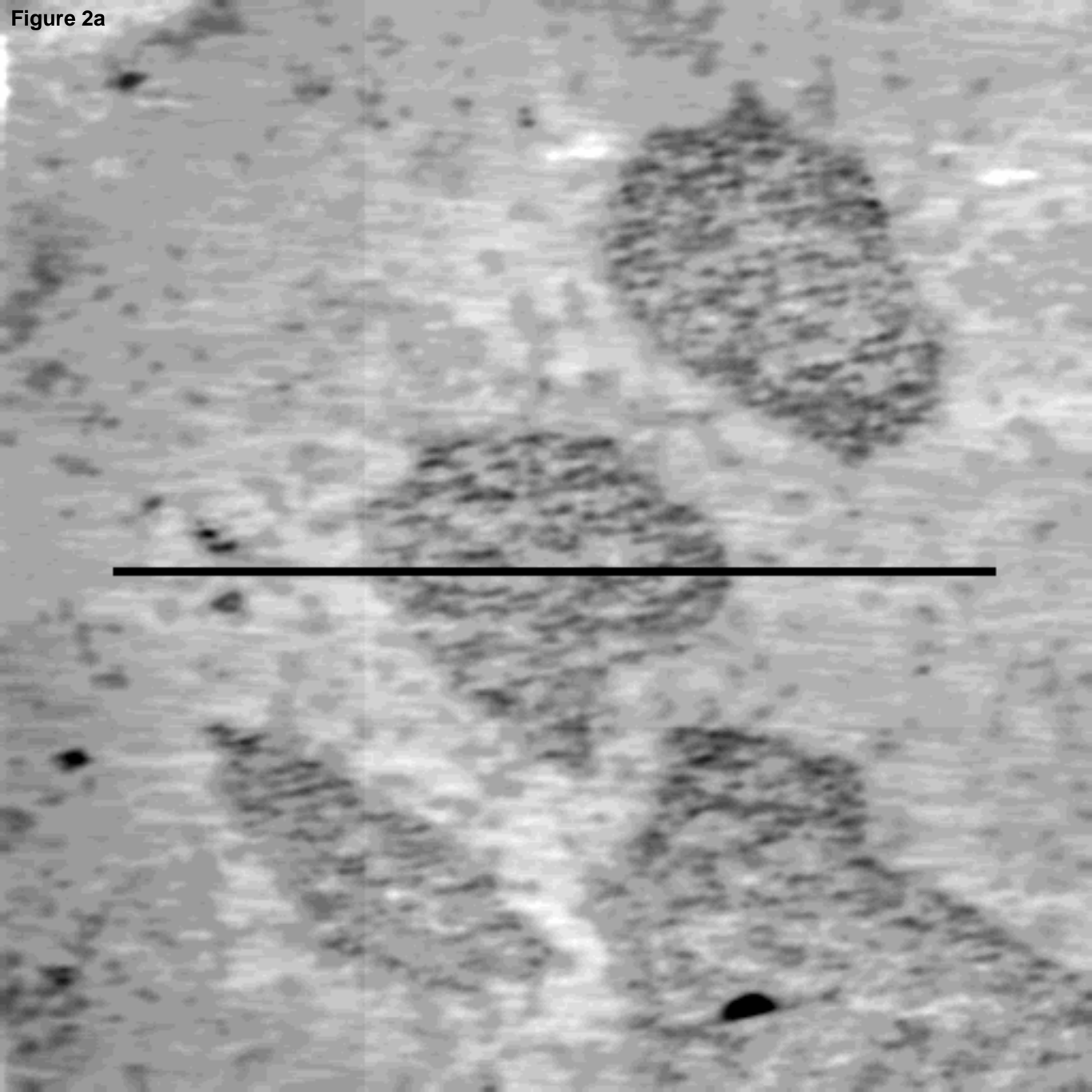
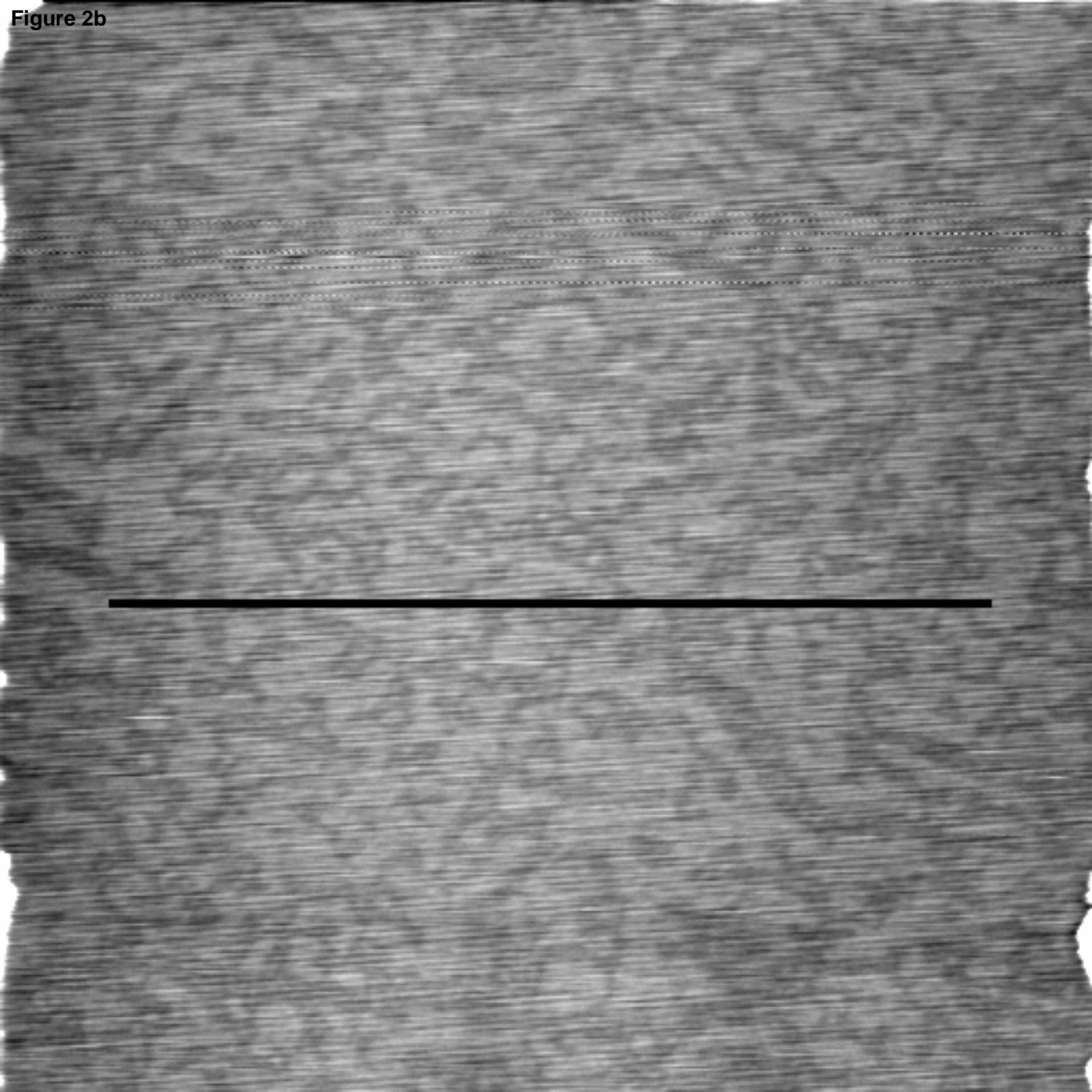
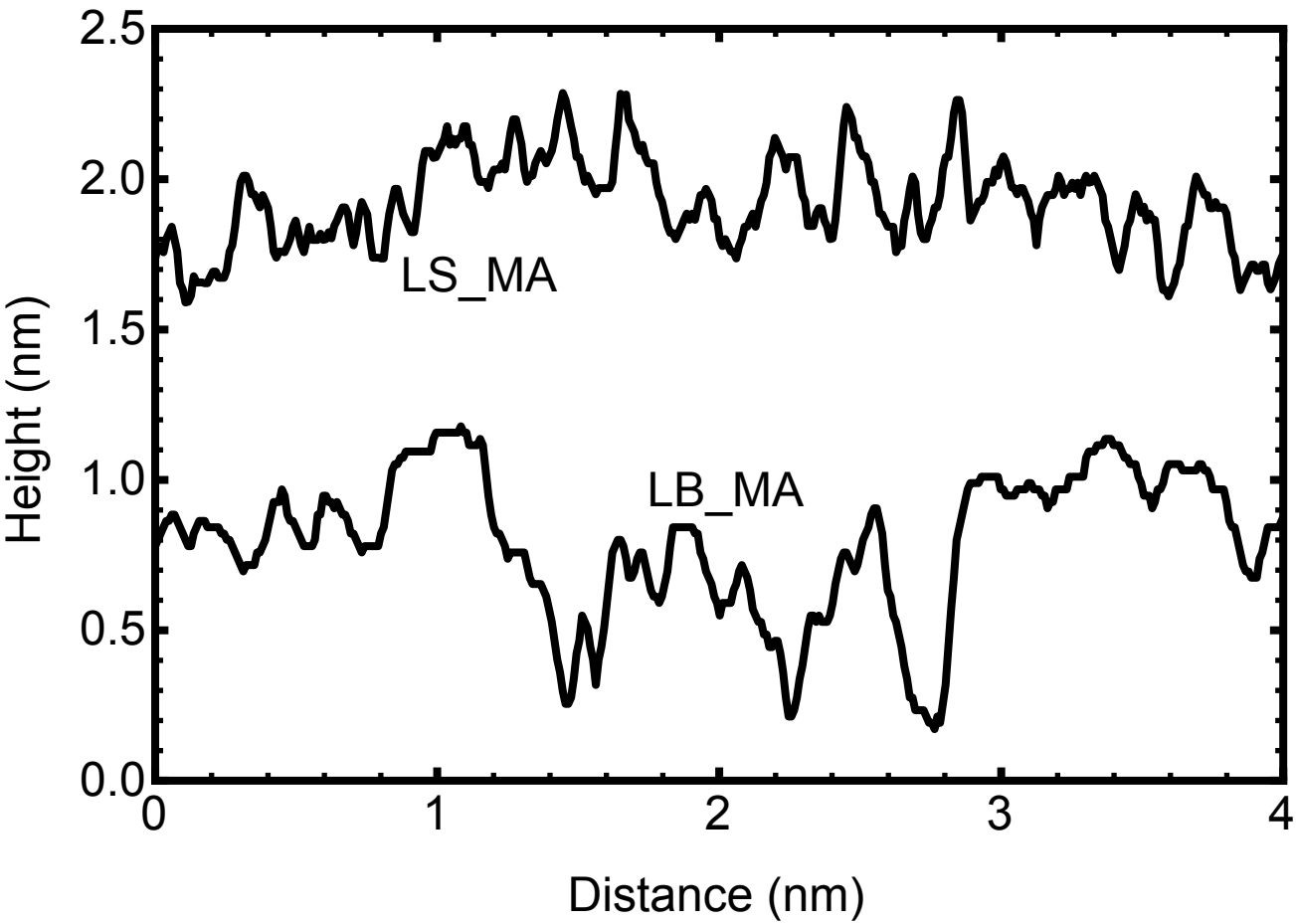


Figure 2b





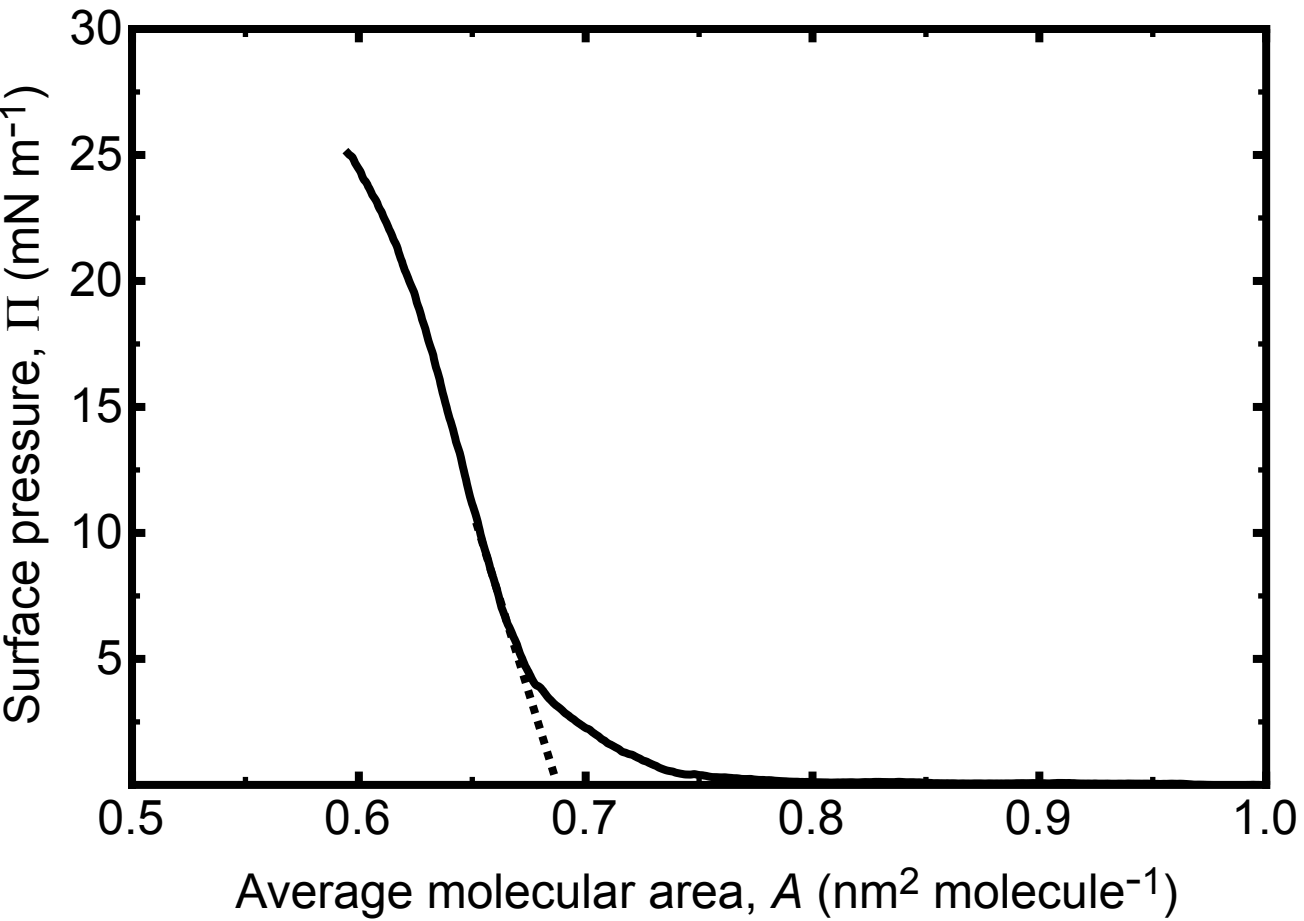
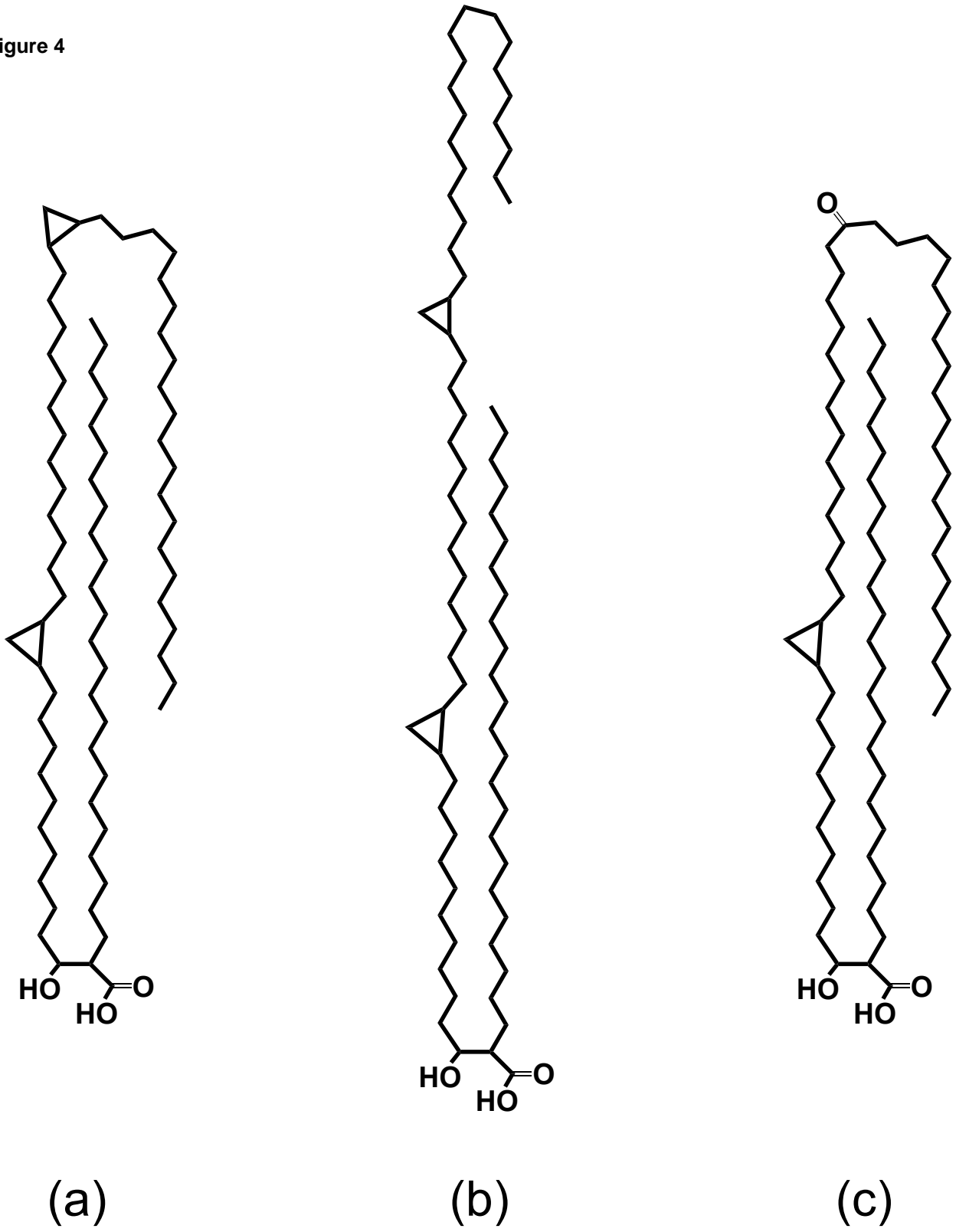
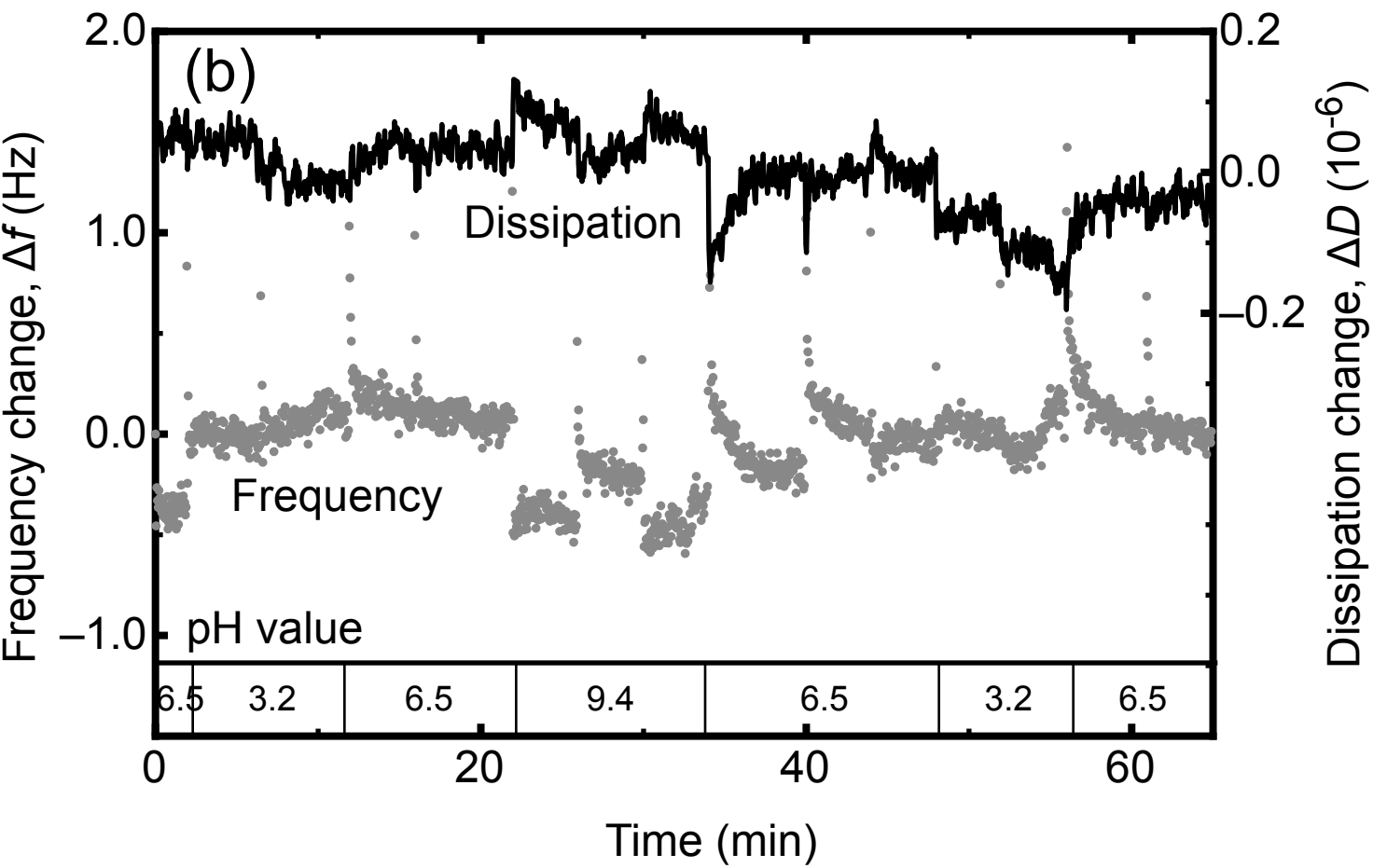
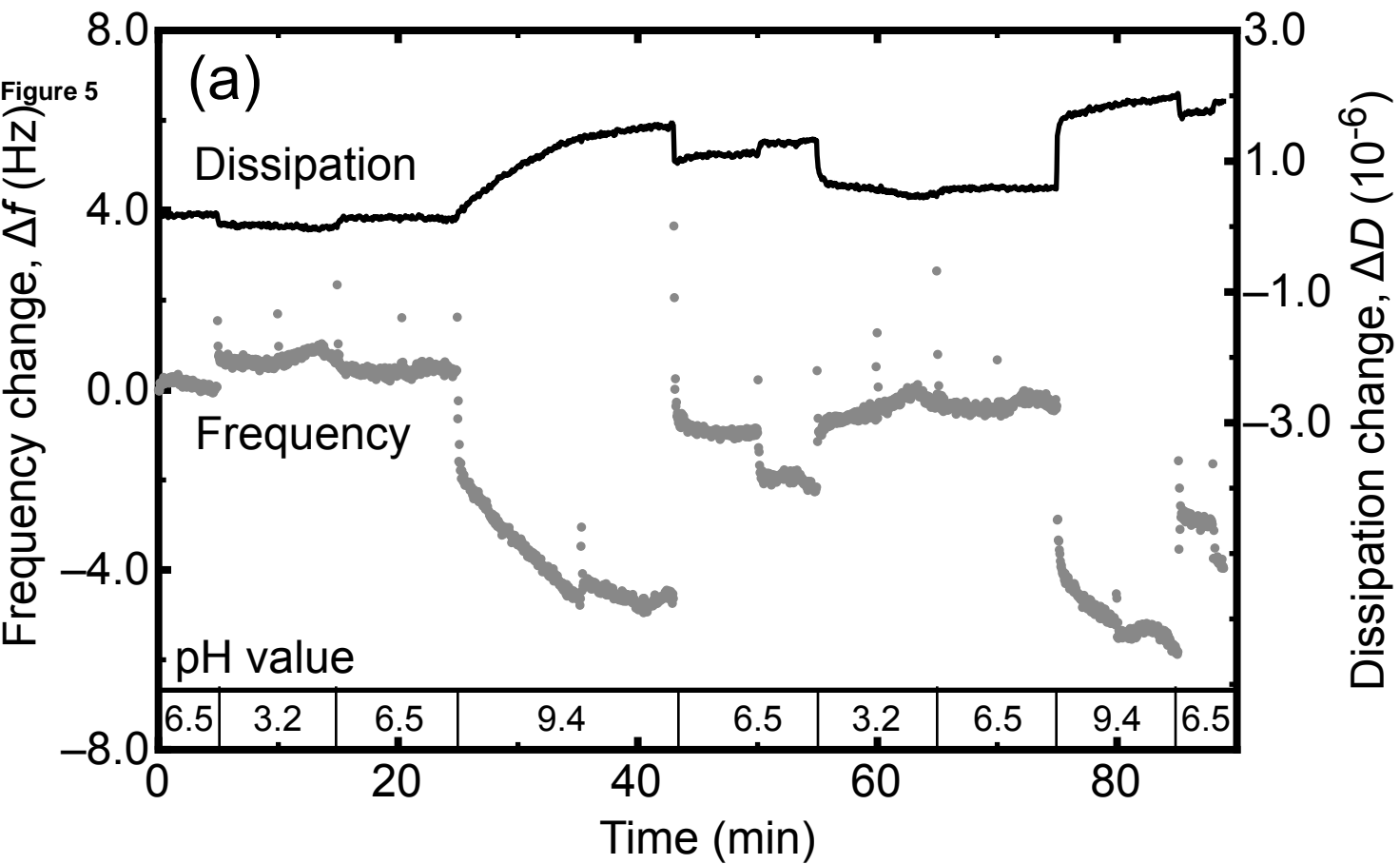
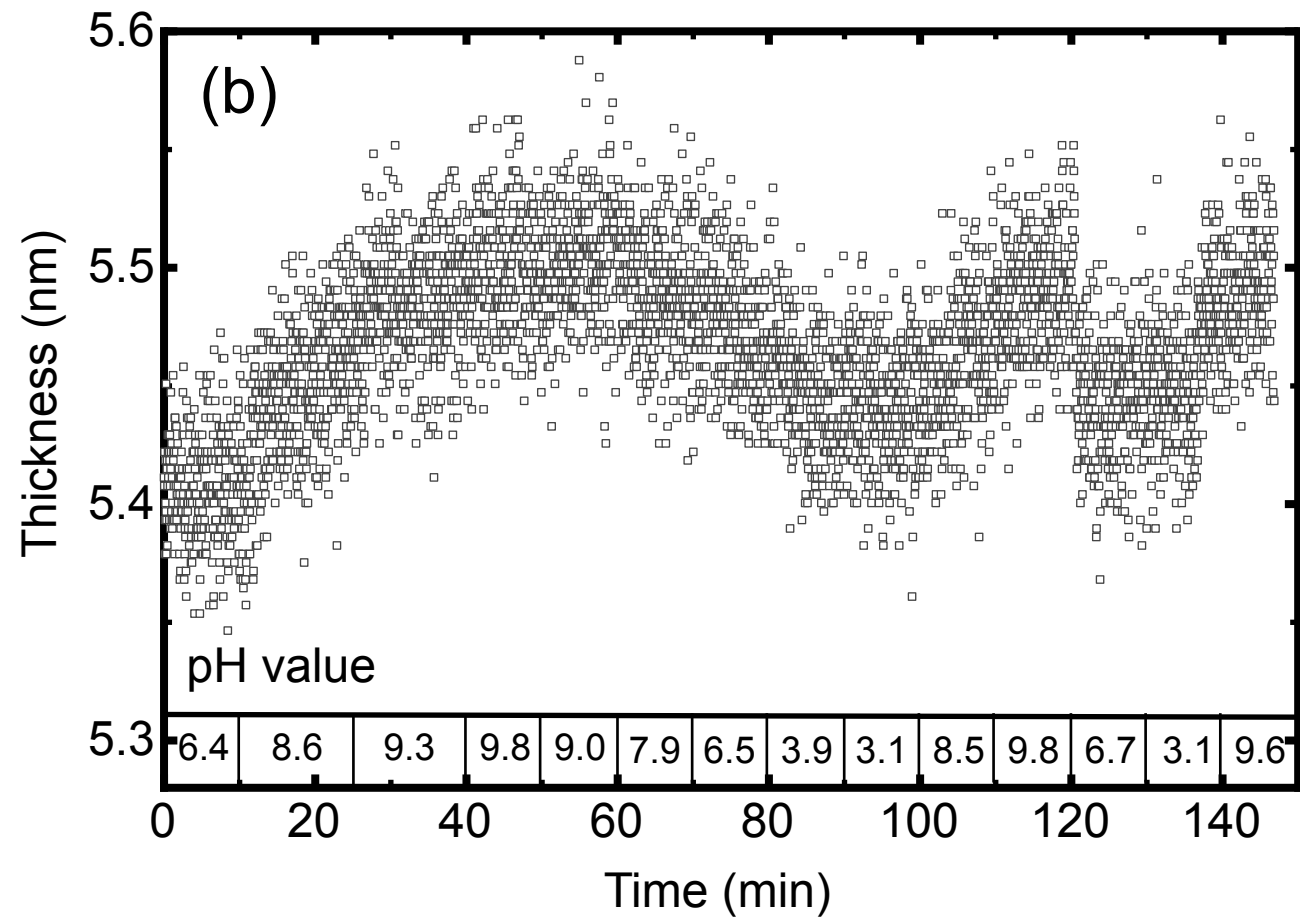
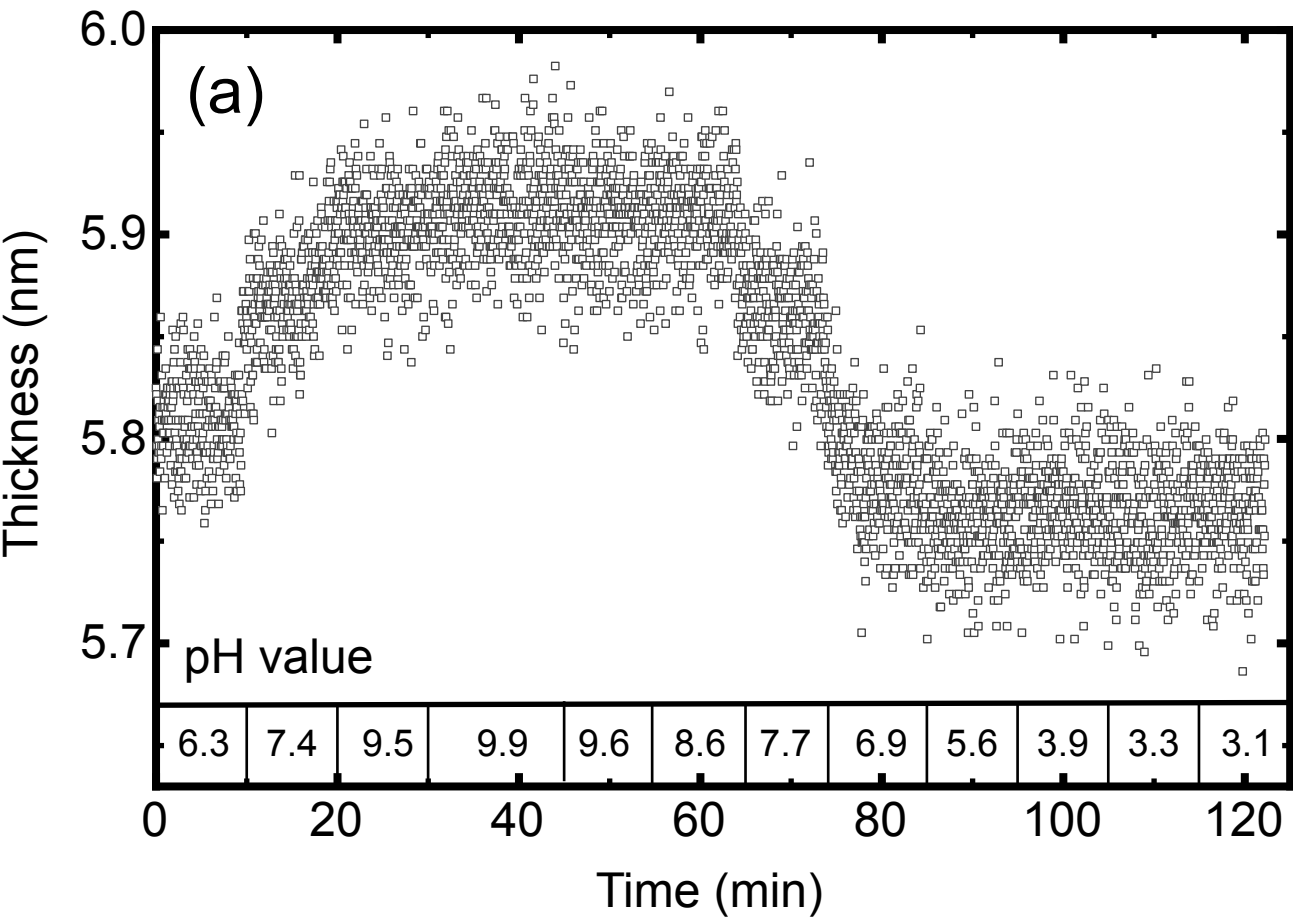
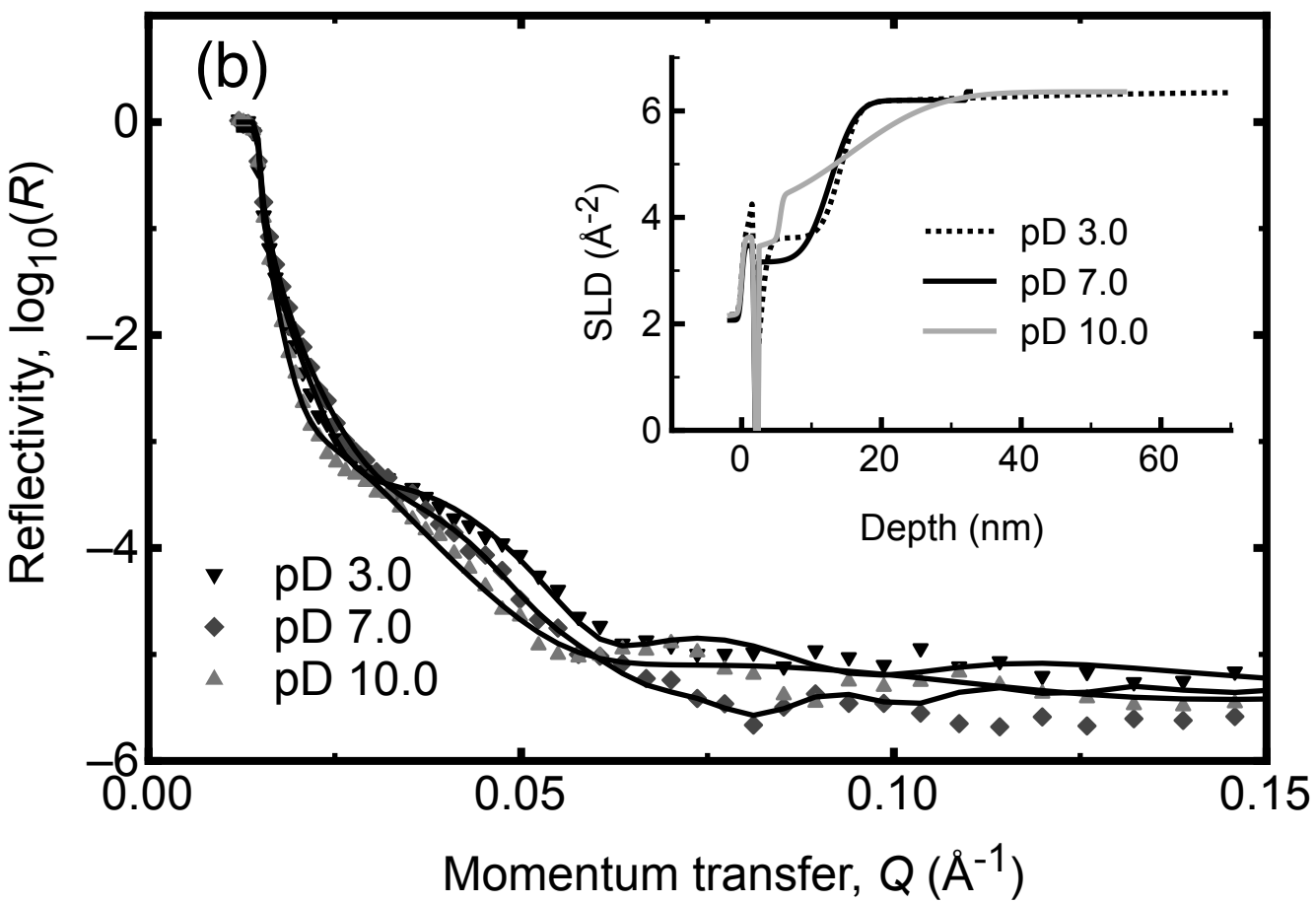
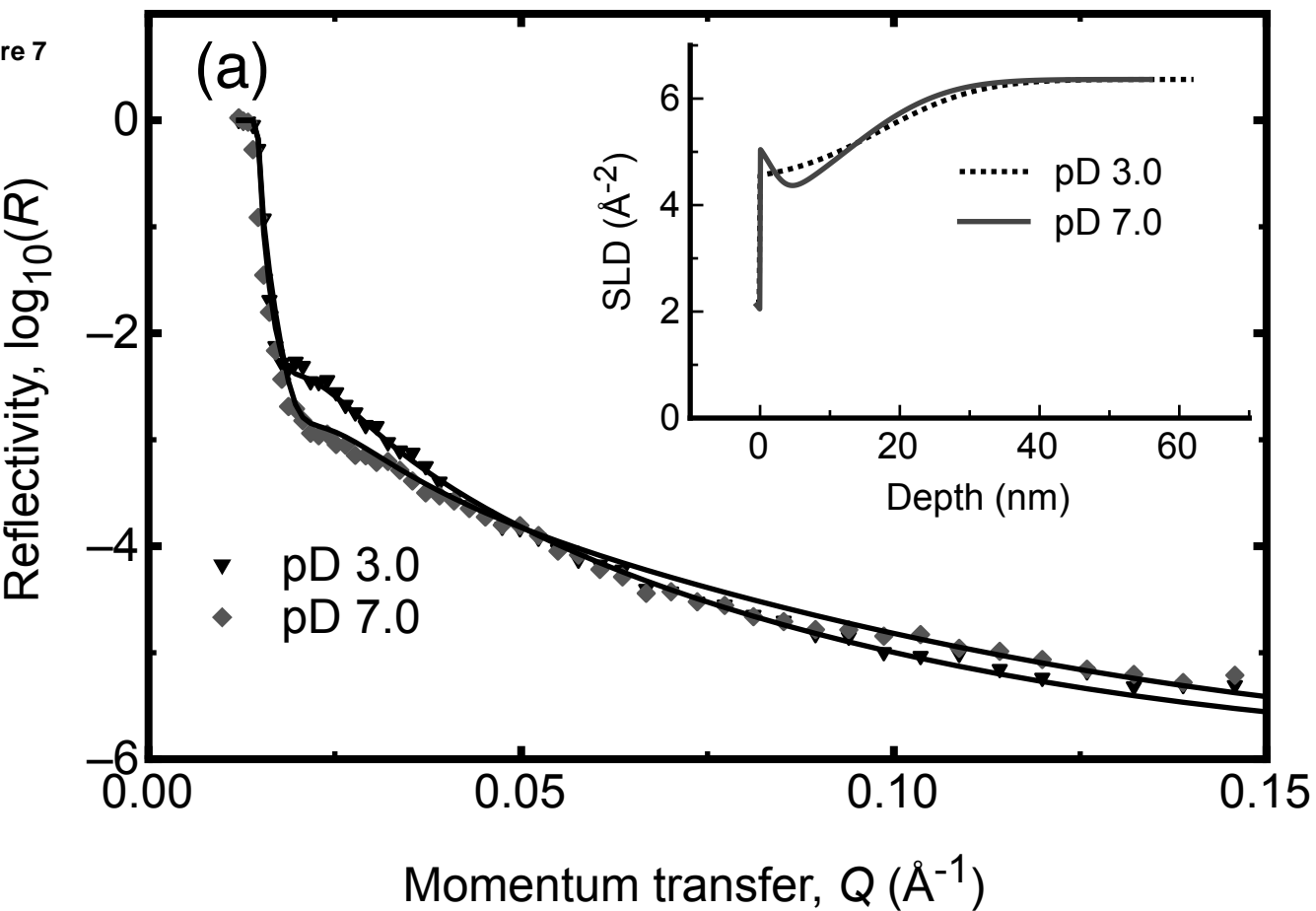


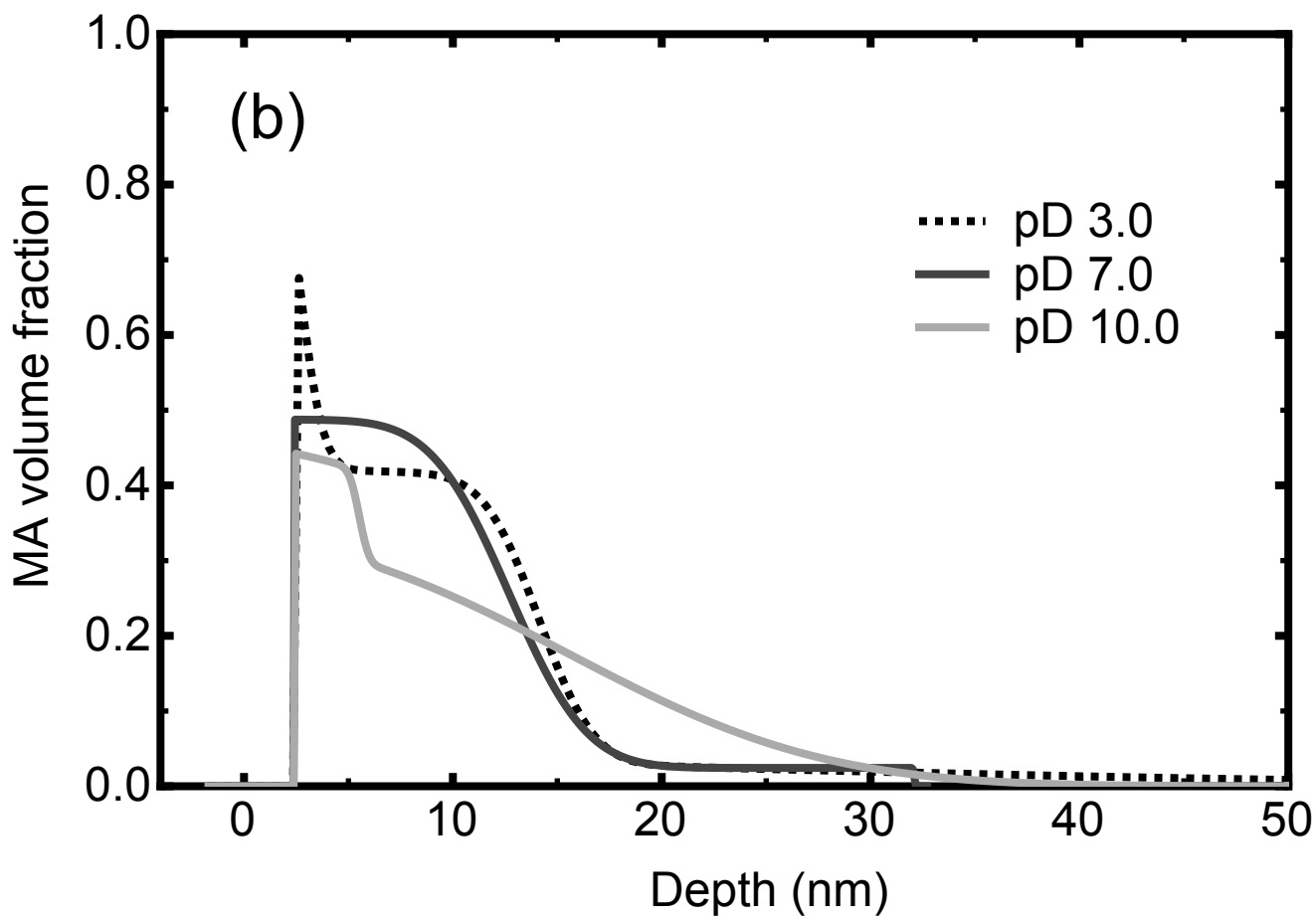
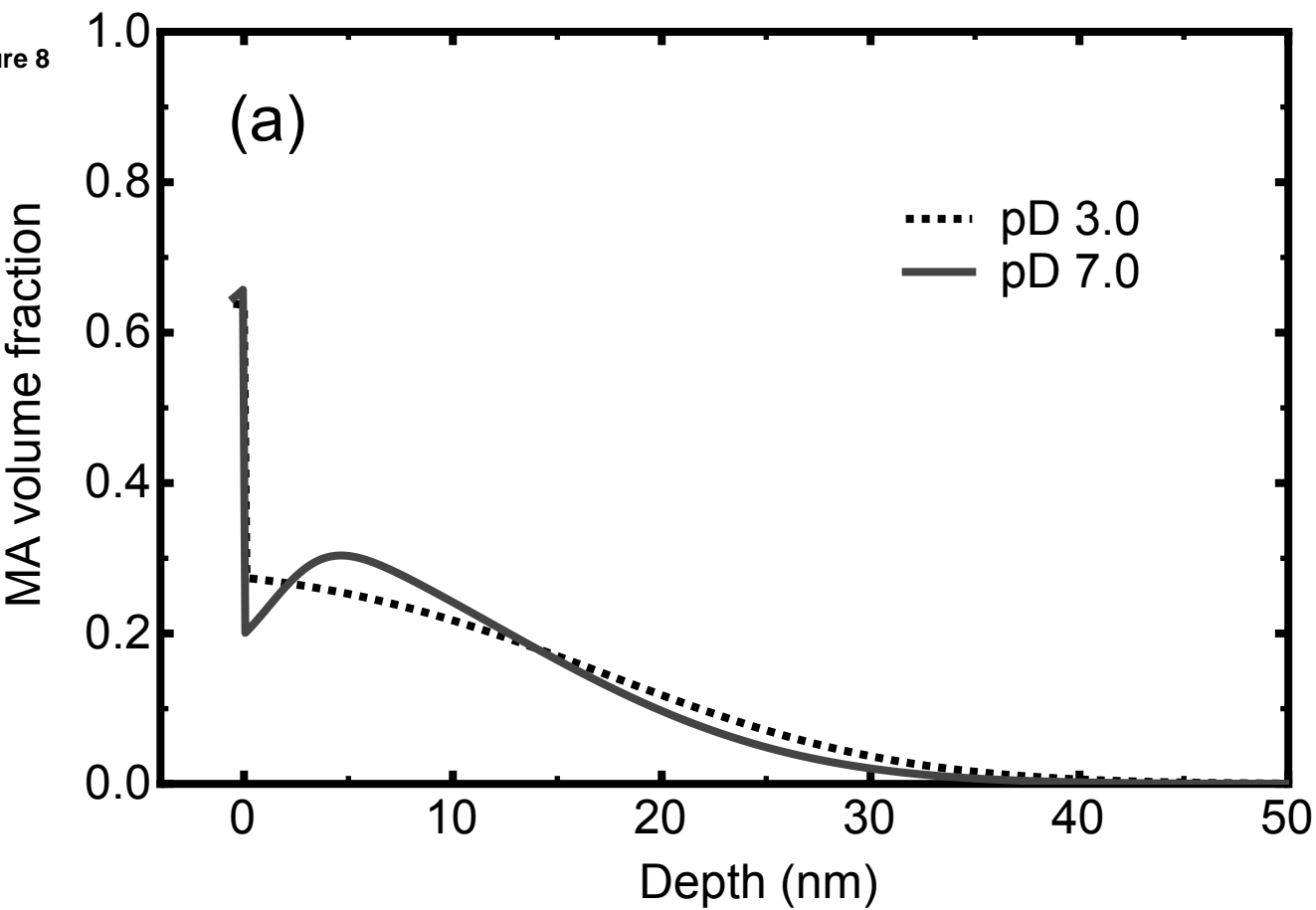
Figure 4

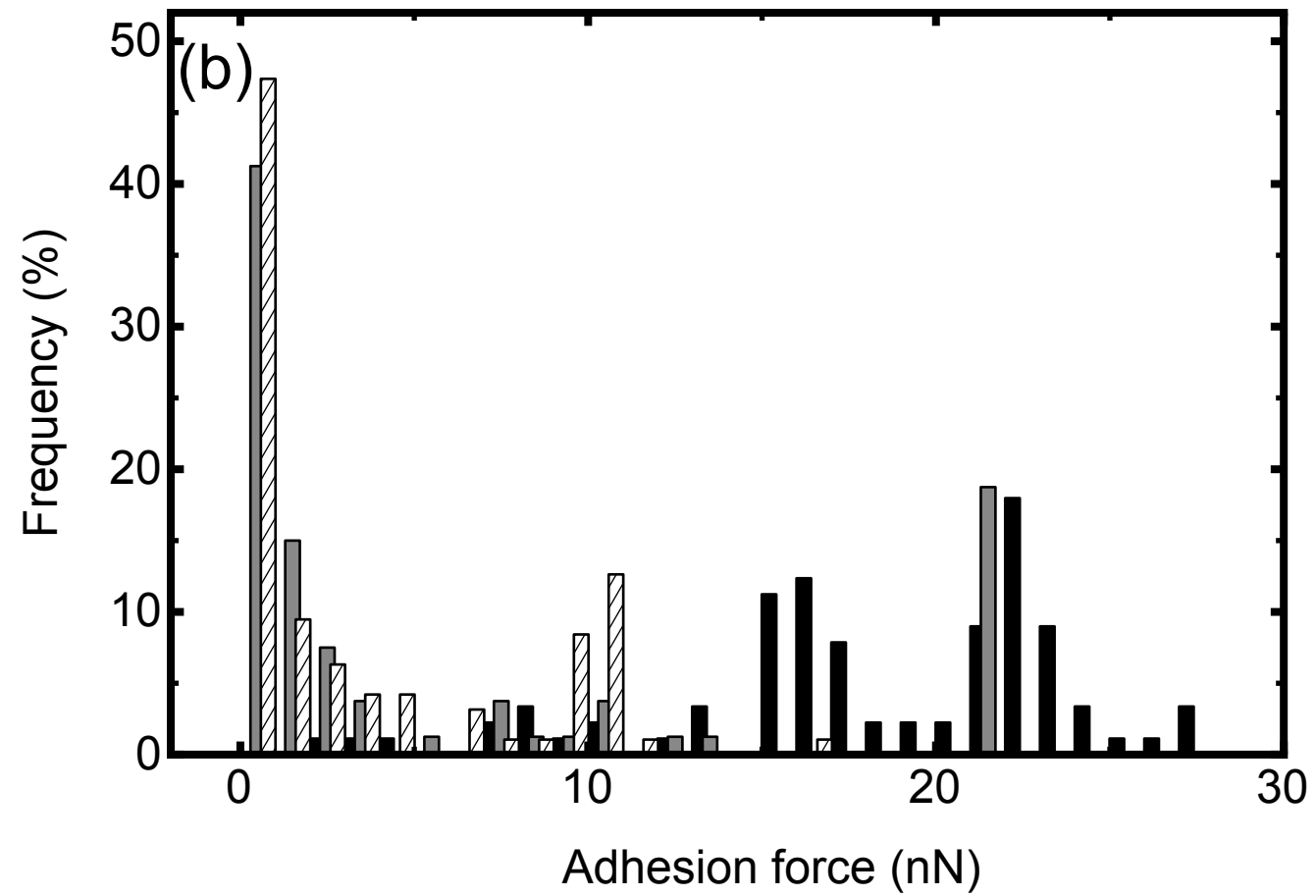
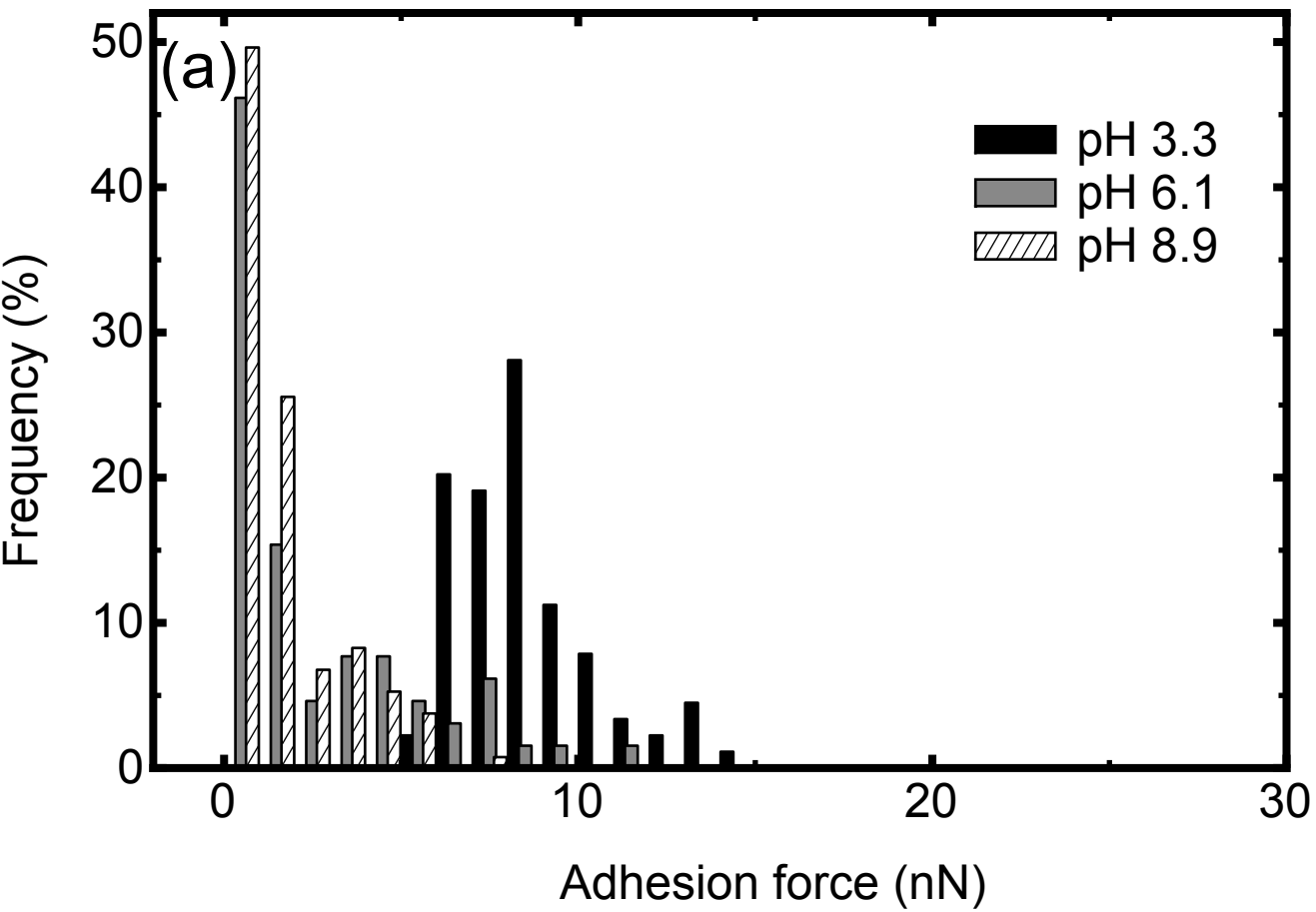


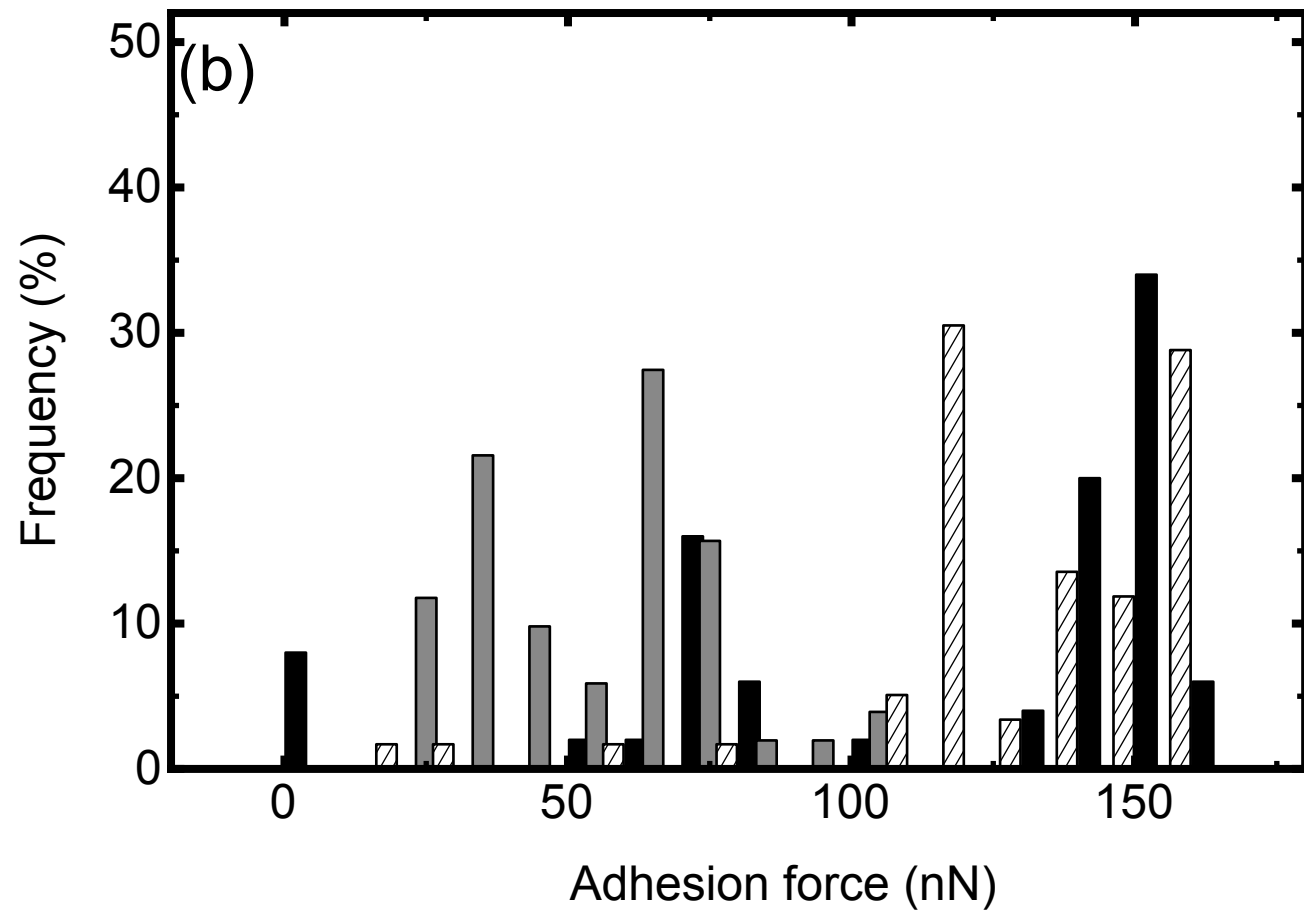
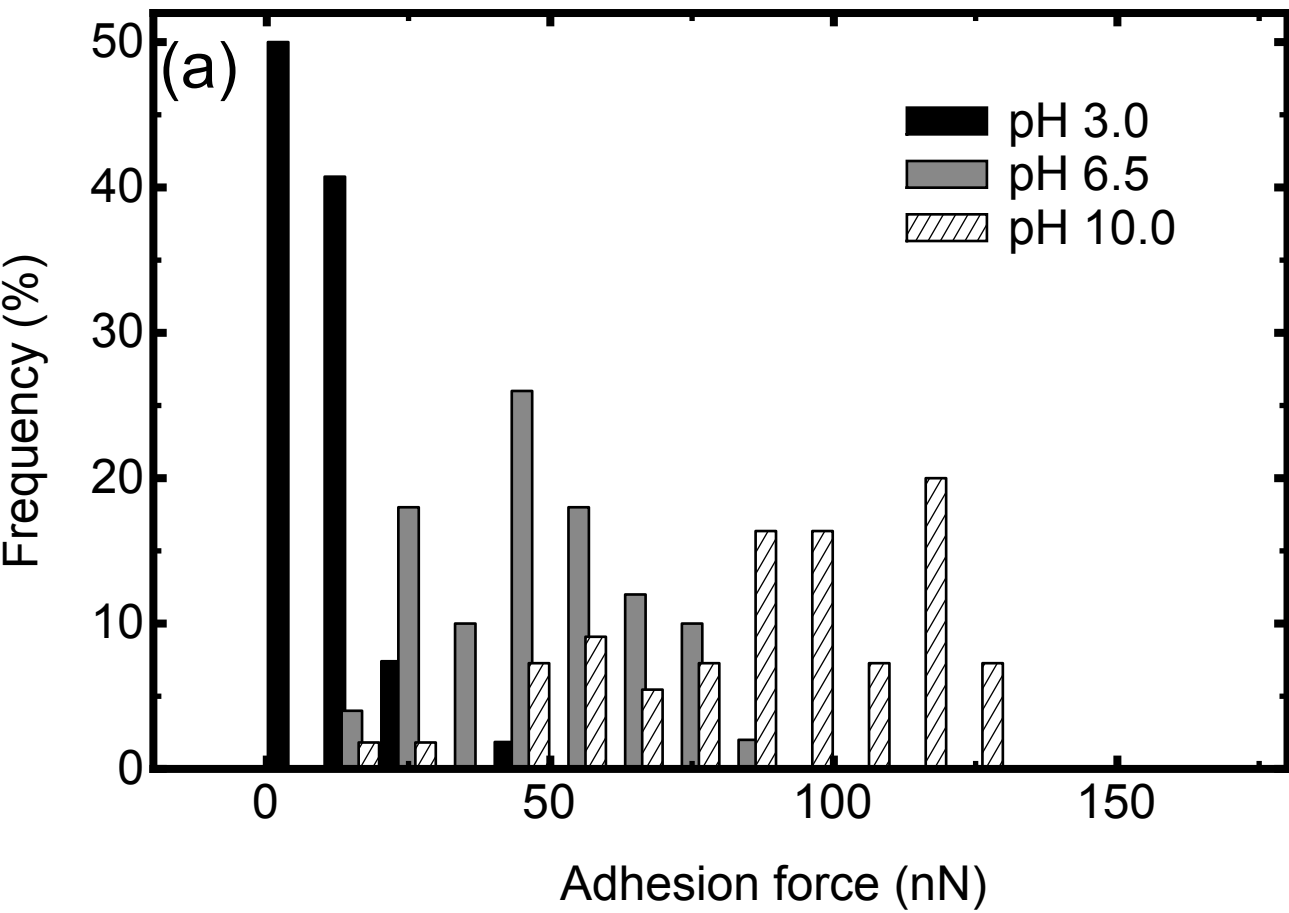


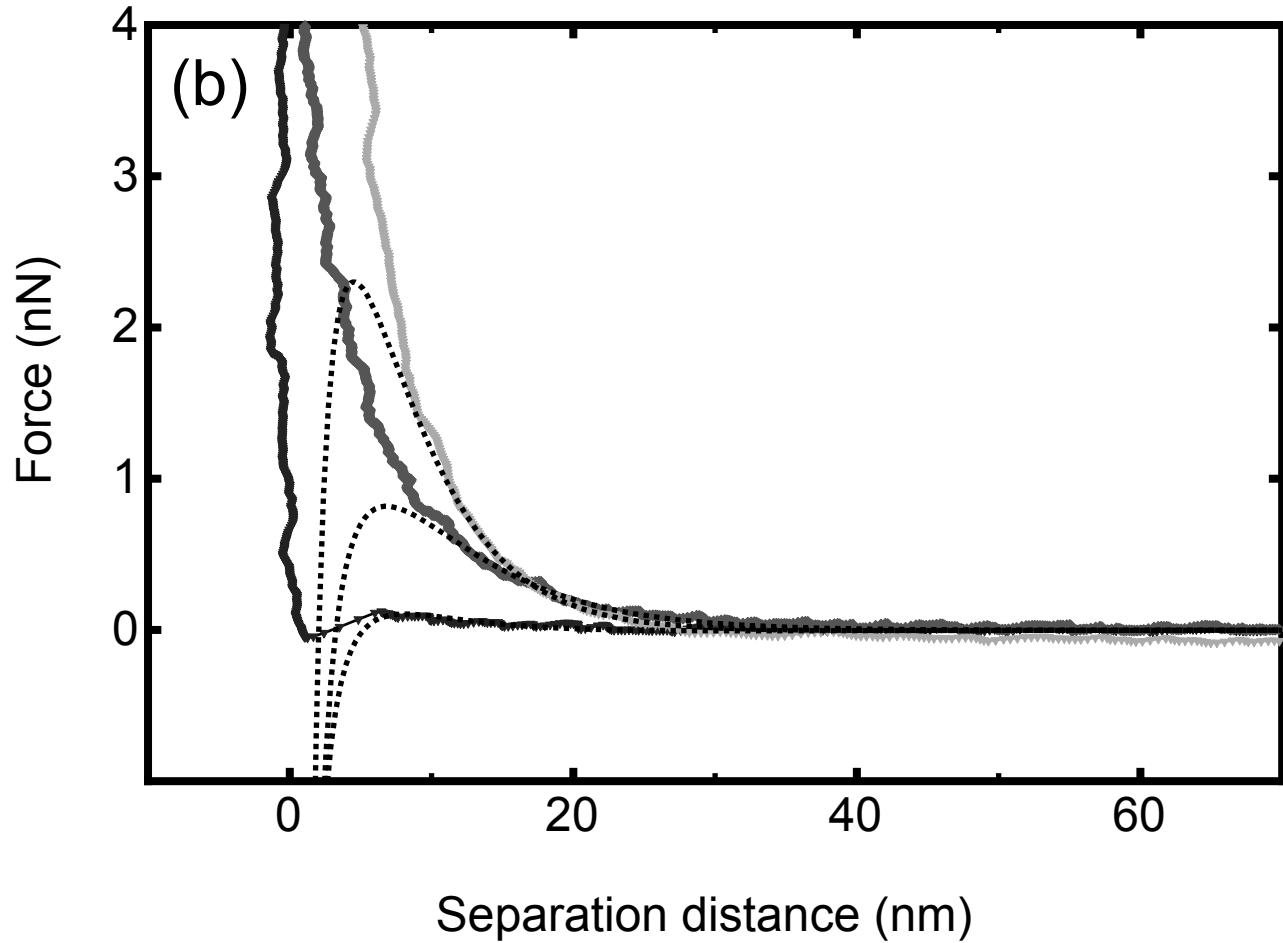
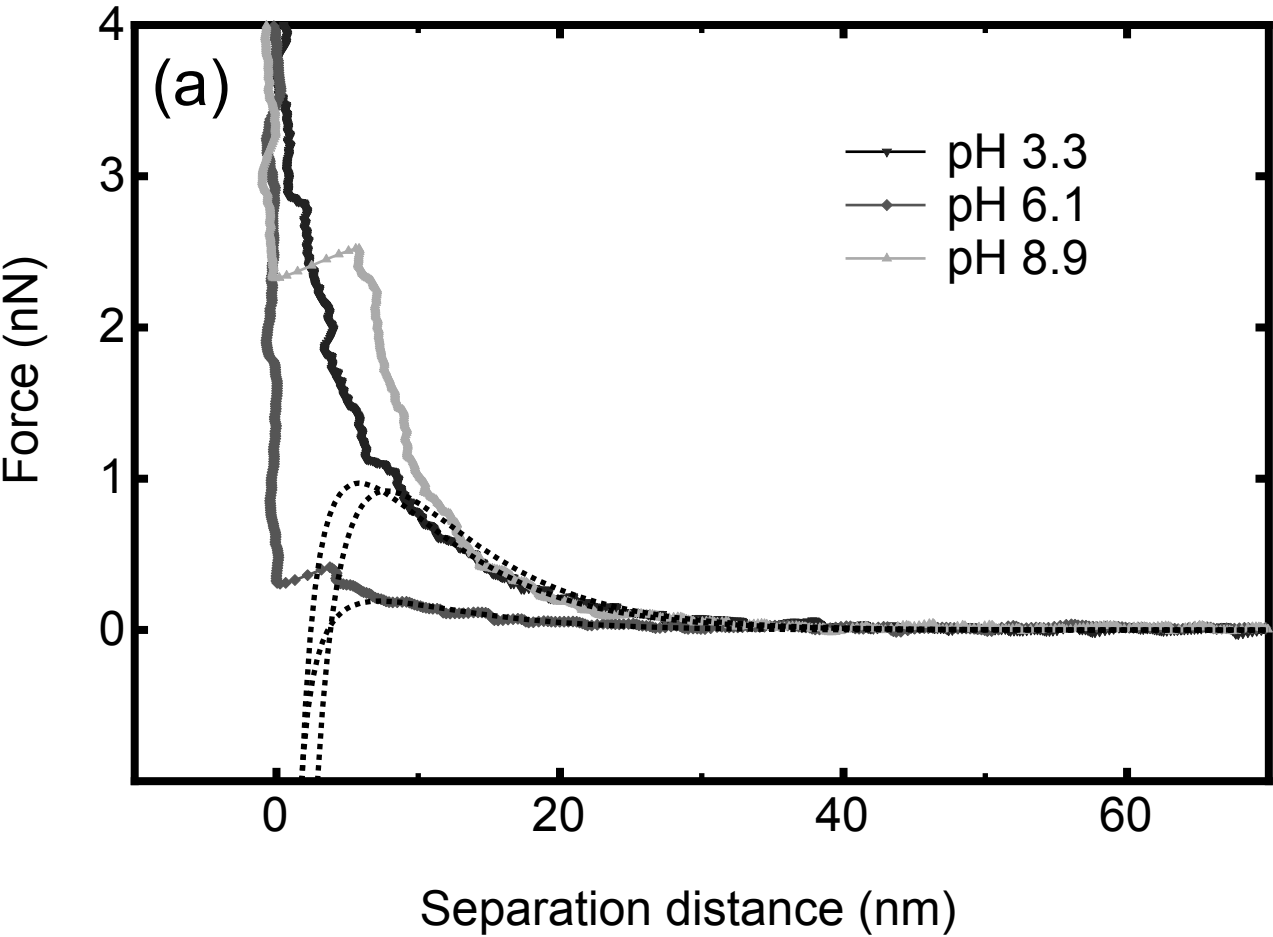












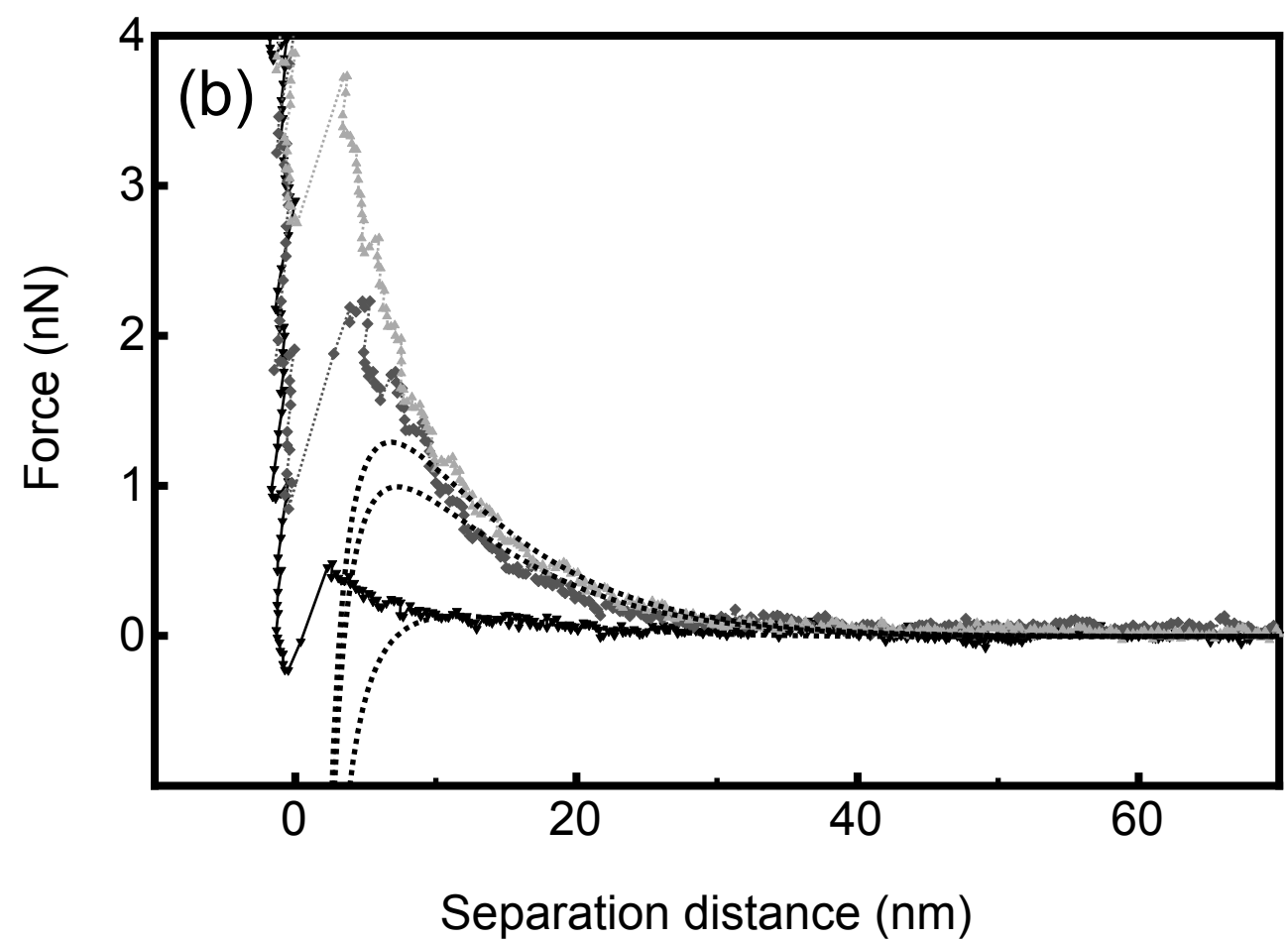
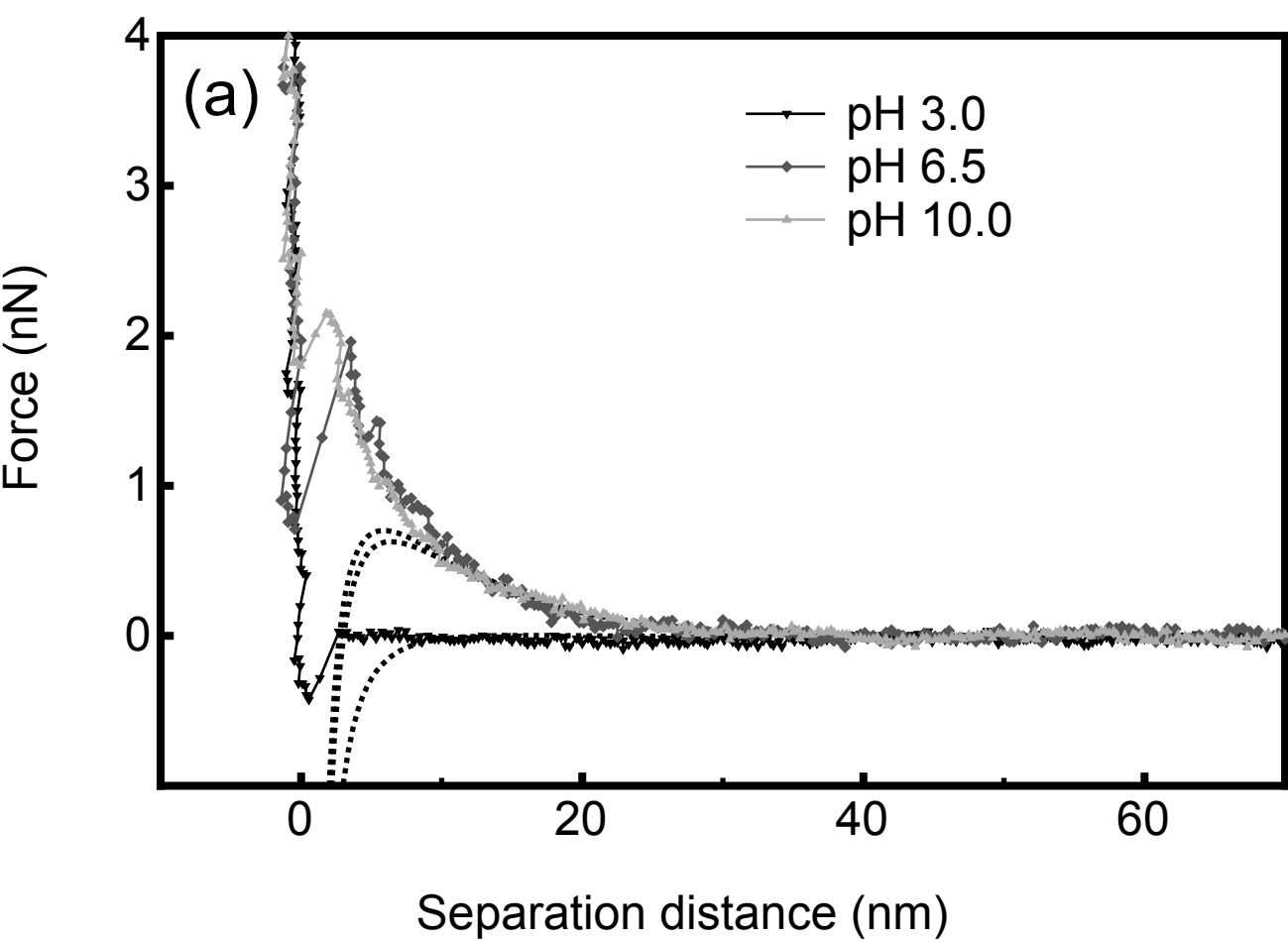
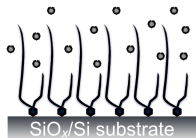


Figure 13

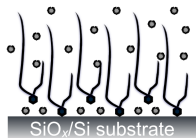
LB_MA

pH 3



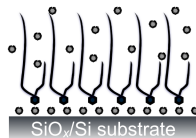
(a)

pH 6



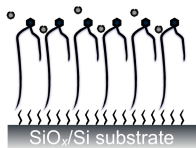
(b)

pH 9

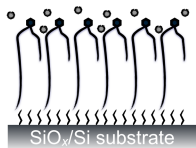


(c)

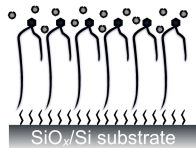
LS_MA



(d)



(e)



(f)



◦ water molecules

⋈ HMDS